TESLA Report 2005-18

WARSZAW UNIVERSITY OF TECHNOLOGY

Faculty of Electronics and Information Technology
Institute of Electronics Systems

Arkadiusz Kalicki

M.Sc. Thesis

The measuring station for research of effects of increased radiation on CCD and CMOS sensors (Radiation Effects on Photonics Devices)

Mentor:

Dr habil. Ryszard S. Romaniuk

Tutors:

Dr Bhaskar Mukherjee, DESY
Dr Stefan N. Simrock, DESY
Dr Krzysztof T. Poźniak, WUT

Warsaw, September 2005

Contents

THE MEASURING STATION FOR RESEARCH OF EFFECTS OF INCREASED RADIATION ON CCD AND CMOS SENSORS (RADIATION EFFECTS ON PHOTONICS DEVICES)

This work comes into being as a part of projects, realized by PERG[1] group in cooperation with DESY (Deutsches Elektronen – Synchrotron) in Hamburg, Germany.

There are two new projects being developed. X-FEL – X-ray Free Electron Laser and VUV-FEL – Vacuum Ultraviolet Free Electron Laser. The new idea is to place some electronic control systems in collider tunnel, where during operation a dose of neutron and gamma parasitic radiation is produced. Exposure to increased radiation may cause many problems in regular work of electronic devices.

The goal of this diploma work was to perform irradiation sensitivity experiments of electronic components, especially CCD and CMOS sensors. As well development of low cost and real time measurement methods of radiation level using those sensors and neutron bubble detectors.

Study of radiation influence on electronics components was done, physics aspects of possible effects and methods of recognition and counting. There were developed proper algorithms used for CCD and CMOS cameras and image recognition algorithm for reading neutron bubble detectors – Optical Bubble Counting Algorithm (OBCA) with user friendly graphical interface written in JAVA. This paper presents developed algorithms, scheme of measurement and results.

[1] Science group, working in Institute of Electronic Systems at Warsaw University of Technology, abbreviation for Photonic Engineering Research Group.

Chapter 1

Introduction

For research in natural sciences photons ranging from radio frequencies to hard γ-rays and including visible light, ultraviolet radiation and X-rays provide the most important tool to study nature. From these, X-rays, discovered in 1895 by C.W. Röntgen, have been used for many fundamental discoveries and outstanding applications which were rewarded with many Nobel Prize Awards. They have played a crucial role in basic science and medical diagnostics, as well as in industrial research and development. The main reason for this success is that the X-ray wavelength, which determines the smallest distance one can study with such a probe, is comparable to the atomic dimension.

In spite of the efforts made in building more powerful X-ray tubes, their progress was only moderate for a long time, it was finally made with synchrotron radiation sources. Synchrotron radiation (SR) has provided over the past thirty years an increase in flux and brilliance by more than ten orders of magnitude. Of course, this opened up fundamentally new areas of research.

However, even with these types of brilliant sources, all electrons emit their radiation field without a fixed phase relation leading to an incoherent superposition. The technical challenge was therefore to introduce a constant phase relation between the electrons traveling through an accelerator structure. Already in 1951 was shown that an electron bunch traveling through an undulator magnet array can amplify radiation. Later developments in 1960 and 1970 started technology called the "free electron laser" (FEL). The idea of self amplified spontaneous emission (SASE) opened the path to build an FEL as a source for X-rays. Researches in the early 1990s showed that very long undulators coupled to linear accelerators can provide coherent X-rays with true laser properties [1].

The X-FEL[1] and VUV-FEL[2] projects at TESLA[3] Technology being developed at DESY[4] in Hamburg, Germany is continuation of therse researches [18], [27], [25]. The X-FEL facility will be built using niobium superconducting cavities, producing moderate dose of neutron and gamma parasitic radiation during operation. The new idea is to place some electronic control systems in collider tunnel, near superconducting cavities. Exposure to increased neutron and gamma radiation may cause many problems in regular work of electronic devices [18], [19].

Main troubles are due to ionization and displacement damage of semiconductors. Influence on the electronic systems by the radiation could happen single event upsets, flipping bits in memory, total ionizing dose effects and limited life time of electronics [5], [4].

There is a need of experiments to study the radiation sensitivity of electronic components. These tests should provide the information needed to optimize the design of electronics for VUV-FEL and X-FEL to minimize failures during its operating, as well low cost and real time measurement methods of radiation level are needed to be develop.

1.1 Accelerators at DESY

DESY – Deutsches Elektronen Synchrotron is located in Hamburg, Germany. The arial view of DESY is shown on **figure 1.1**. There are various accelerators, the biggest HERA is 2 *km* diameter. The entire DESY is located within the PETRA Ring, 750 *m* diameter. Location plan of major DESY accelerators is shown on **figure 1.2**. The description of the accelerators is presented in **table 1.1** and **table 1.2** [19], [26].

1.1.1 X-FEL – X-Ray, Free Electron Laser

The XFEL X-ray laser will open up new applications for research. Its very high-energy, short-wave X-ray light will provide previously unknown insights. The facility will make it possible to film molecules during chemical reactions or to depict molecules which in the past were too small for imaging techniques or which could not be fixed. In the field of physics, it will enable the study of the material state of a gas plasma [28], [32].

X-ray light is already being used today to examine the tiniest structures. It has led to important new findings in chemistry, biology, materials research and physics. Nevertheless, examinations of complex biomolecules for example, which are of interest for the treatment

[1] X-ray Free Electron Laser.
[2] Vacuum Ultraviolet Free Electron Laser.
[3] Tera Electron Volt Superconducting Linear Accelerator.
[4] Deutsches Elektronen – Synchrotron, Hamburg, Germany.

Accelerator	Dimension	Particle Specification
HERA	2 *km* diameter	e/e+: 12 => 27.5 GeV/c p+: 40 => 920 GeV/c
PETRA II	730 *m* diameter	e/e+: 7.0 => 12 GeV/c p+: 7.5 => 40 GeV/c
DORIS III	95 *m* diameter	e/e+: => 4.5 GeV/c
DESY II	93 *m* diameter	e/e+: 450 MeV/c => 7.0 GeV/c (PETRA) e/e+: 450 MeV/c => 4.5 GeV/c (DORIS)
DESY III	101 *m* diameter	p+: 310 MeV/c => 7.5 GeV/c (PETRA)
LINAC II	70 *m* length	e/e+: 7.0 => 450 MeV/c
LINAC III	32 *m* length	p+: => 310 MeV/c
PIA	9.5 *m* diameter	e/e+: => 450 MeV/c
TTF II	250 *m* length	e: => 1.2 GeV/c (at present 450 MeV/c)

Table 1.1: Brief description of the major DESY Accelerators.

Acronym	Explanation
HERA	Hadron Elektron Ring Anlage
PETRA	Position Elektron Tandem Ring Anlage
DORIS	Doppel Ring Speicher
LINAC	Linear Accelerator
PIA	Positron Intensity Accumulator
TTF	TESLA Test Facility

Table 1.2: Explanation of the acronyms.

of diseases, still require a great deal of effort and expense. Nor is X-ray light suitable for observing chemical reactions in real time. The XFEL X-ray laser will now make it possible to enter whole new dimensions. The abbreviation XFEL stands for "X-ray free-electron laser".

Electrons will be accelerated to very high energy levels in the XFEL and stimulated to emit X-ray light with special properties. The wavelength of this X-ray light is so short that even atomic details are recognizable. It can be varied in the range between six and one tenth nanometers - that is a billionth of a meter [33].

At peak values, its brilliance is a billion times higher than that of the most modern X-ray light sources, and its average brilliance is 10,000 times higher. This will enable the examination of entire new classes of molecules [1].

Its time resolution is several times better than that of the light sources available today: An X-ray flash is shorter than 100 femtoseconds (thousand billionth of a second). That is the amount of time it takes for chemical compounds to form and groups of molecules to change their position. This will make it possible to more or less "film" chemical reactions. In addition

Figure 1.1: The Arial View of DESY Research Centre [19].

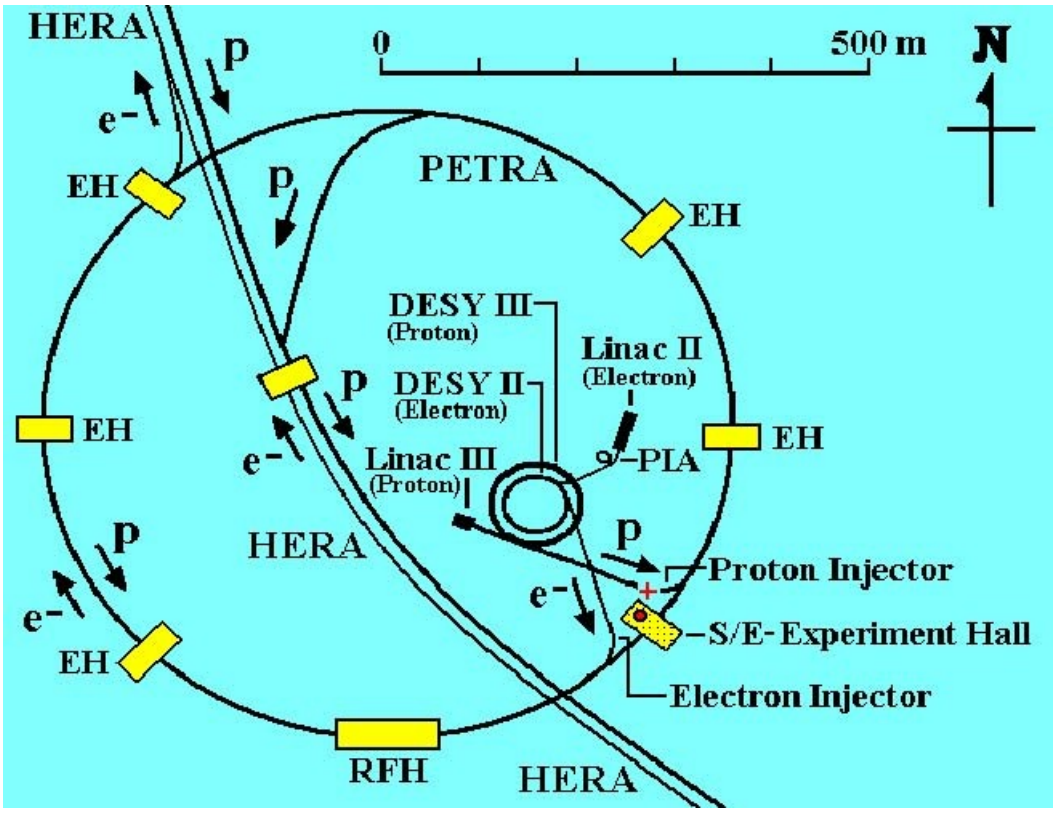

Figure 1.2: Location plan of major DESY Accelerators [19].

the light flashes will have the properties of laser light and thus enable, for example, three-dimensional images of the nanoworld or holographic experiments at the atomic level. The technology for the construction of the XFEL is based largely on the preliminary work of the German Electron Synchrotron DESY. The accelerator elements for the XFEL were developed in the course of this project and the laser principle for the X-ray laser tested. Only recently, a smaller free-electron laser for longer wavelengths was successfully commissioned at the DESY. Among other things this will enable technical studies with regard to the realization of the XFEL [28].

The X-ray laser is planned as a European project with close links with DESY. The 3.3 kilometre-long X-ray laser XFEL is to be located in the federal states of Hamburg and Schleswig-Holstein. It will begin on the DESY site in Hamburg-Bahrenfeld and end in the neighbouring town of Schenefeld (district of Pinneberg), where the experimental hall with ten measuring stations is to be erected [32].

So far 10 countries (France, Denmark, Germany, Greece, Italy, Poland, Spain, Sweden, Switzerland and Great Britain) have signed a Memorandum of Understanding for the preparatory phase of the project. Hungary, the Netherlands, Russia and the EU are also observing the project's progress. The cost of building the XFEL is currently estimated at approximately 934 million euro. The BMBF is working on the assumption that it will provide up to 50% of the funding, the federal states of Hamburg and Schleswig-Holstein 10%, and the international partners the remaining 40% [28].

Providing the further preparations and construction work proceed according to plan, the XFEL could be commissioned in 2012.

Radiation from a Free Electron Laser (FEL) has much in common with radiation from a conventional optical laser, such as high power, narrow bandwidth and diffraction limited beam propagation. One of the main differences between the two lasers is the gain medium. In a conventional LASER[5] the amplification comes from the stimulated emission of electrons bound to atoms, either in a crystal, liquid dye or a gas, whereas the amplification medium of the FEL are free (unbound) electrons. The free electrons have been stripped from atoms in an electron gun and are then accelerated to relativistic velocities [35].

1.2 Influence of radiation on electronics components

Because of mechanism and caused effects they can be generally divided into three groups [5], [15], [18]:

- Total Ionizing Dose (TID):

[5]Light Amplification by Stimulated Emission of Radiation

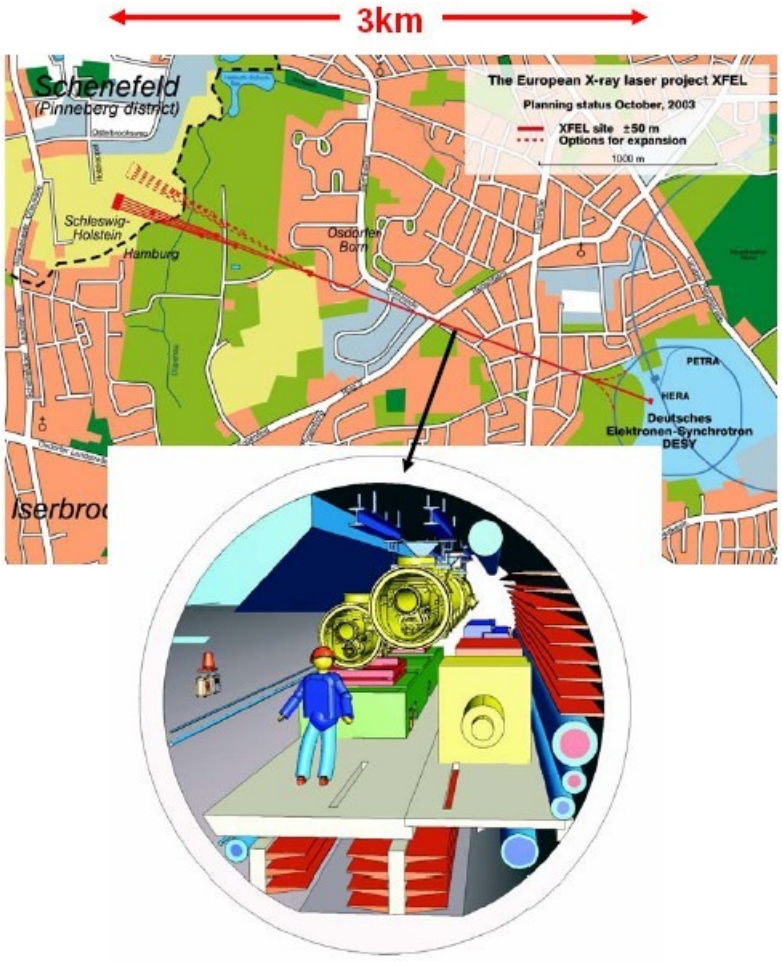

Figure 1.3: XFEL project on Hamburg map [32].

Caused by neutrons, protons, heavy particles, gamma. It is degradation and/or failure as a function of ionizing radiation accumulation.

- Single Event Effects (SEE):

  Caused by neutrons. It is relatively instantaneous device upset or destruction (latch-up, burnout, gate rupture).

- Displacement damages:

  Caused by heavy and secondary particles. It is the result from particles producing Non Ionizing Energy Loss (NIEL).

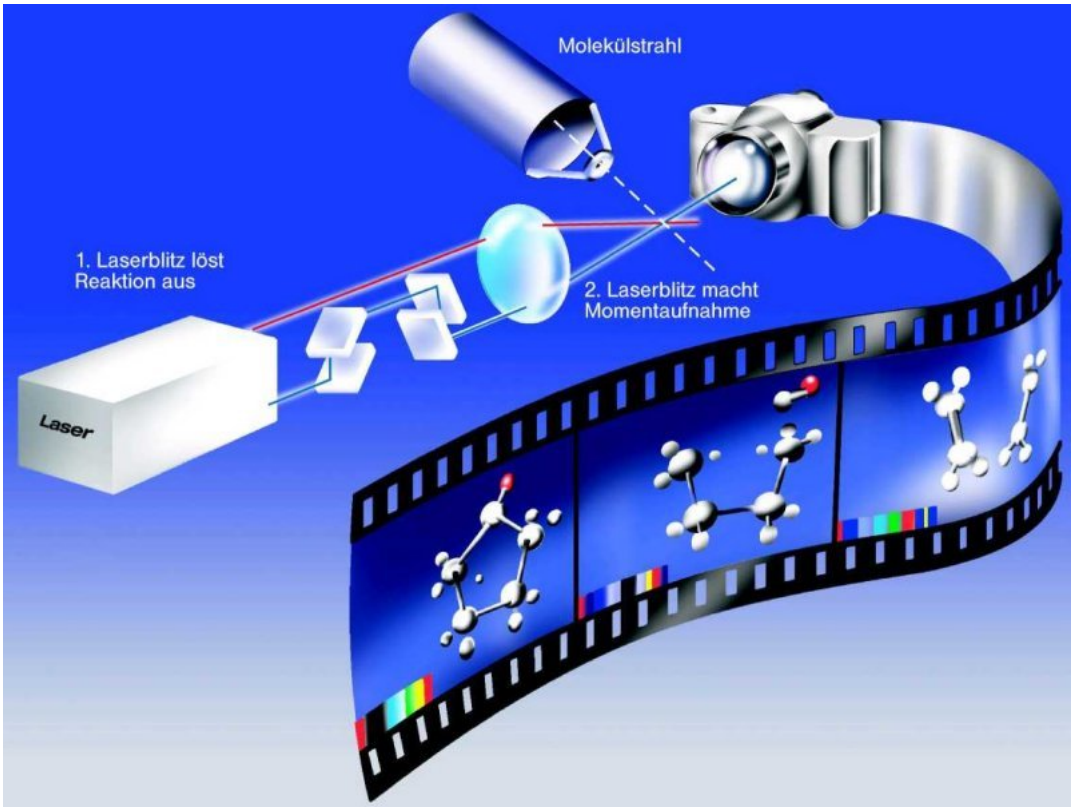

Figure 1.4: Making movie of chemical reaction [36].

1.2.1 Total Ionizing Dose

Ionizing radiation causes electron-hole pairs creation in oxide. Some of these pairs recombinate, more if there is no electric field. All left electrons, because of their high mobility leave the oxide. Left holes, because of their very low mobility are mostly trapped. As the result there is positive charge trapped in the oxide [5].

1.2.2 Single Event Effects

Single highly ionizing particle (incident or secondary ion) flies through the oxide. It provokes high electron-hole pairs density along its track and transient current across the oxide. In the result oxide breakdowns. There can be different categories of Single Event Effects [4]:

- Non-destructive results:
  - Single Event Upset (SEU) - bit flips in memory
  - Single Event Functional Interrupt (SEFI) - SEUs in device control logic (eg. in FPGA: JTAG TAP controller, Select Map interface)

  - Single Event Transient (SET) - changes in propagated signal

- Destructive results:

  - Single Event Gate Rupture (SEGR) – gate-to-channel short circuit
  - Single Event Burnout (SEB) – high instantaneous current — > junction breakdown
  - Single Event Latch-up (SEL) - Vdd-to-Vss short circuit

1.2.3 Displacement Damage

Heavy or secondary particle collides with atoms from crystal structure of the semiconductor material. It causes defects in this structure along the track of particle.

The effects of displacement damage could be [18]:

- minority carrier's lifetime decreases
- carrier's mobility decreases
- effective majority carrier's concentration decreases – resistivity increases
- creation of acceptor levels – type inversion (N — > P)

Chapter 2

Prerequisites and project goals

The goal of the project is to work out an idea, realization and implementation of the measuring station for research on increased irradiation influence on CCD and CMOS sensors. Elaborating and practical application optimized methods of measuring influence accelerator irradiation source on the sensors. As well real time measurement methods of radiation level using CCD (Charge Coupled Device), CMOS camera sensors and Neutron Bubble Detectors.

This work was divided into chapters, first is the introduction, seconds describes assumptions and project goals, next presents project realization: the hardware construction and software algorithms. The next presents the research and shows tests results. Last summarizes the results and describe possible future project development. In appendix there are described radiation and health aspects.

The test took place at DESY (Deutsches Elektronen – Synchrotron) in Hamburg, Germany.

2.1 The experiments to be performed

The experiments where divided into the stages:

1. Investigation of irradiation effects on CCD and CMOS sensors – complete systems:
    - determine Single Event Effects (SEEs) – recorded on camera sensors as "blinking pixels"
    - determine Total Ionizing Dose (TID) effects and displacement damages – observed as permanent white pixels and higher values of dark current
    - predict performance and life-time in VUV-FEL and X-FEL tunnels

2. Radiation level measurements:

   - development model of realtime neutron radiation detector based on CCD camera sensor and calibrate the measurements with other methods (CCD was chosen because it is much more sensitive to radiation damage than other types of semiconductor elements)
   - development of automatic Bubble Neutron Detector reading and real time dose monitoring

3. Radiation prevention methods:

   - tests of different radiation shielding
   - test different shielding configurations.

2.2 Principle of operation and theoretical aspects of radiation induced damages on CCD and CMOS sensors

2.2.1 CCD sensors

Principle of operation

The pixels in CCD sensors are built up by MOS capacitors in which the electrons (number N) generated by photon absorption during the exposure are stored. The maximum number of electrons that can be stored in a pixel is the full well capacity *fwc*. In interline-transfer (IT) and frame-transfer (FT) sensors, the electrons are shifted into separate storage cells at the end of the exposure time *t*. After this shifting, that lasts for several μs for IT sensors and about 1 ms for FT sensors, the next image can be exposed. During the exposure of the next image the charge Ne (e: elementary charge) in the storage cells is shifted pixel by pixel into the sense node (readout node) with capacity C, where it is converted into the output voltage $U = Ne/C$. The node sensitivity S is the voltage generated per electron, it lies in the range of some $\mu V/e$ [9].

Influence of radiation

CCD sensors are much more sensitive to radiation damage than other types of semiconductor elements. Signal charge packets travel over a much longer path before being registered, and the readout method (moving signal row by row from the image area into the output register,

with a subsequent shift in the output register to the output node) increases the time a signal is subject to loss [38], [39], [40].

Structure of a CCD sensor is schematically shown in **figure 2.1**. The epitaxial layer of ~ 20 μm thick is the sensitive region. Since most of the epitaxial layer is not depleted, the signal charge (electrons of e/h pairs) diffuses thermally in the epitaxial layer and spreads over several pixels even for the normal incident particles [9], [39].

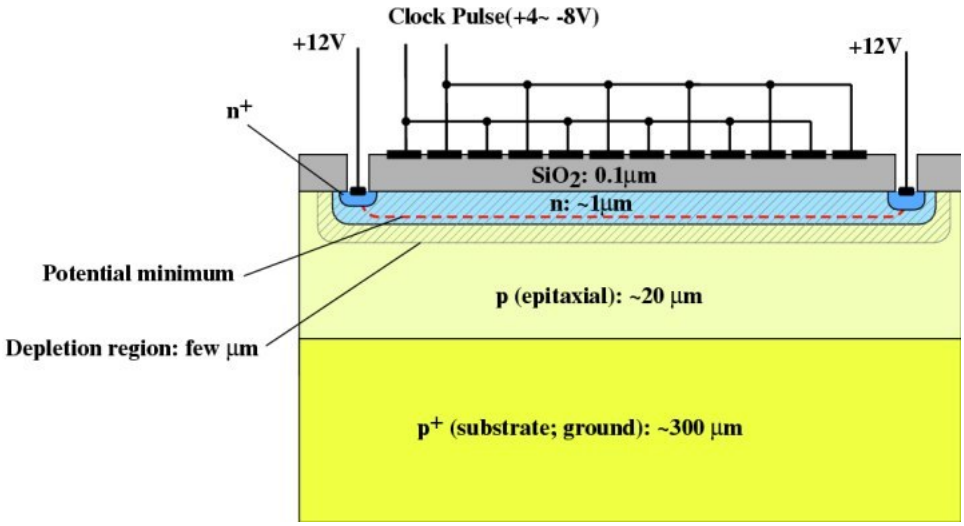

Figure 2.1: Structure of a CCD sensor [9].

Both surface and bulk damage effects are expected to take place in the CCD sensors because of the type and the energy spectrum of the radiation background. Ionizing radiation creates electron-hole pairs in silicon dioxide, which is used as gate and field dielectric in CCDs. Charge carriers drift in the electric field (externally applied or built-in) to the corresponding electrode. Electrons quickly reach the positive electrode, but some of the holes remain trapped in the oxide and give rise to radiation-induced trapped positive oxide charge, which can be stable for long time. At any Si-SiO_2 interface there are a number of interface traps, which result from the strained or dangling silicon bonds at the boundary between the two materials. Ionizing radiation causes the density of these traps to increase, generating radiation-induced interface traps. The formation of radiation-induced trapped oxide charge (or flat band voltage shift) and interface traps is referred under the term **surface damage**.

Radiation with sufficiently high energy can displace Si atoms from their lattice positions, creating displacement damage. This process affects the properties of the bulk semiconductor and is known as **bulk damage**. Low energy electrons and X-rays can deliver only small energy to the recoil Si atom and mainly isolated displacements, or point defects, can be created. On the other hand, heavier particles, such as protons and neutrons can knock out silicon atoms which have sufficient energy to displace other atoms in the crystal. The secondary

displacements form defect clusters, which have high local defect density and can be tens of nanometers wide [15].

Interface traps are the dominant source of dark current in modern CCDs, because the generation rate at the Si-SiO_2 interface is usually higher than that in the epitaxial bulk silicon. Increase of the surface dark current is the main effect expected from radiation-induced interface defects.

Radiation-induced bulk defects cause the dark current in CCDs to increase. Irradiation with heavy particles (e.g. protons, neutrons) often creates large non-uniformities in the dark current spatial distribution in the CCDs. These non-uniformities, also known as “dark current spikes” or “hot pixels” manifest themselves as pixels with much higher dark current than the average value for the CCD (see **figure 2.3** and **figure 2.2**). Their presence has been connected with the high electric fields caused by the device architecture and field-enhanced emission, the cluster nature of the radiation damage and crystal strains in the silicon material [15].

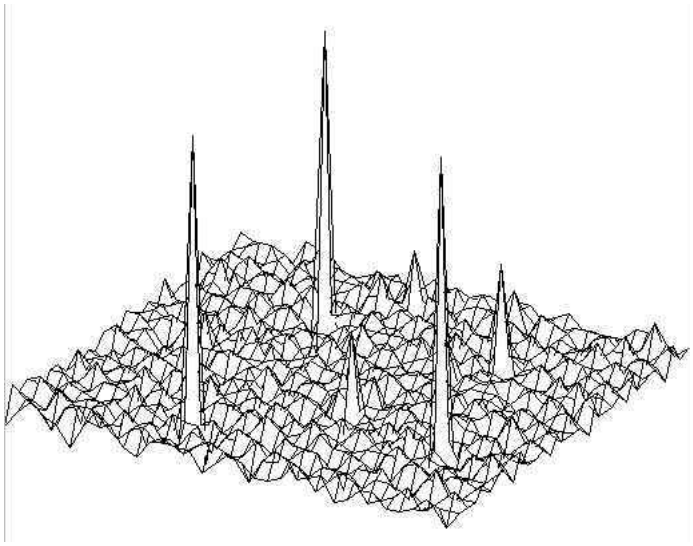

Figure 2.2: Hot pixels 3D.

2.2.2 CMOS sensors

Operation principle

In CMOS sensors the single pixels are built up by photodiodes (see **figure 2.4**). The pixel contains a reset switch, a photodiode, a source follower and a selection switch. The photodiode junction can be the n-well/p-substrate junction of a standard CMOS process. A small junction area can be used to obtain a high sensitivity and a high fill factor. The capacitance

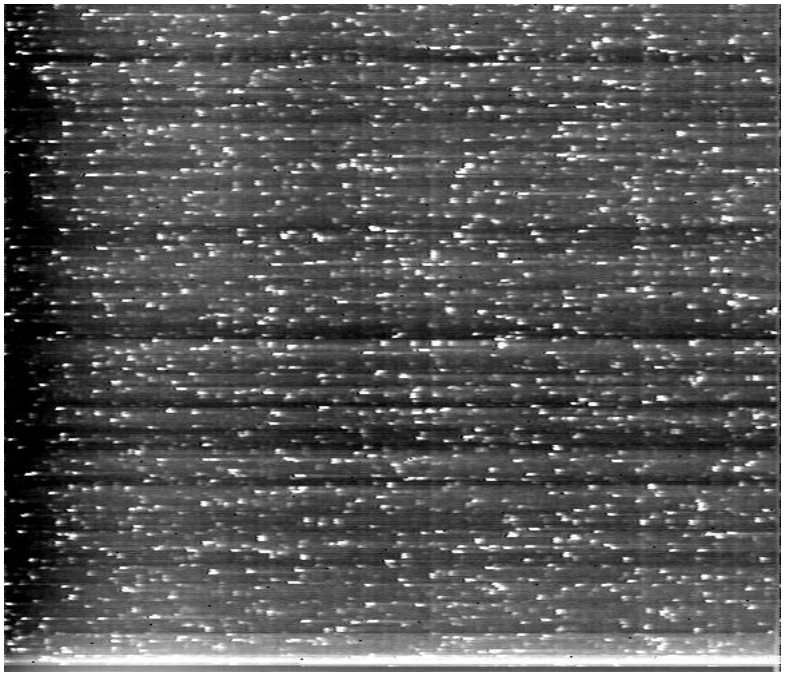

Figure 2.3: Hot pixels image.

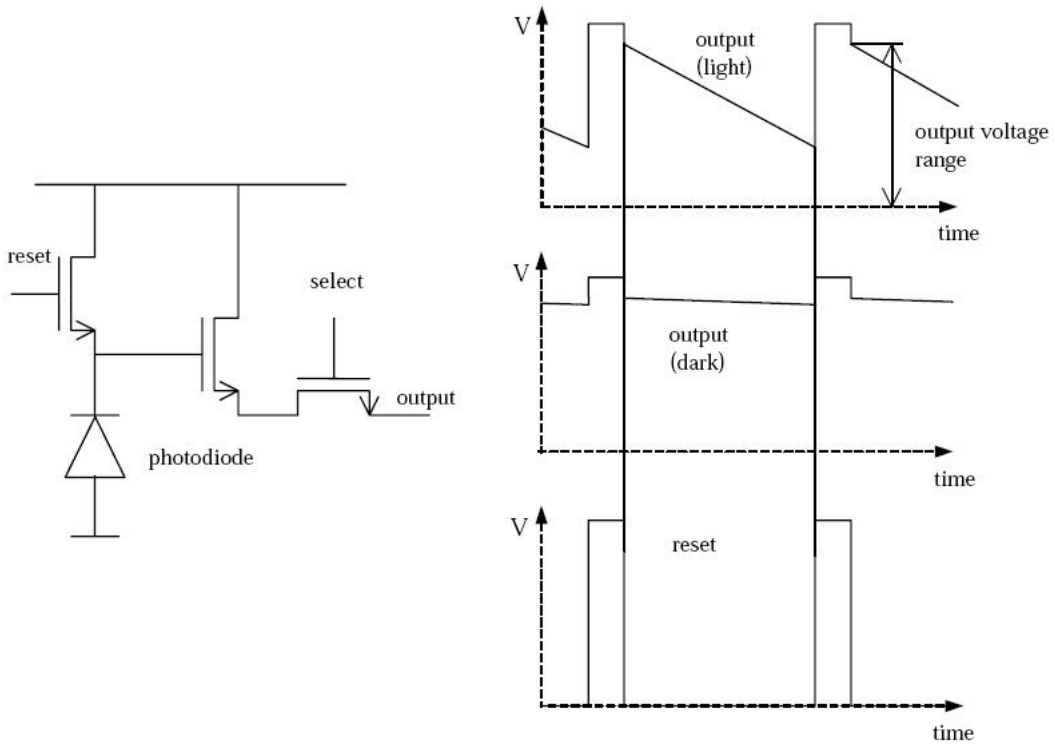

Figure 2.4: Operation principle of CMOS sensor [12].

of the photodiode determines the sensitivity of the pixel. The smaller the capacitance, the higher the voltage swing for each collected charge [37].

When a reset pulse is applied, the junction capacitance of the photodiode is charged to a known value (limited by the threshold voltage of the reset transistor). The integration starts when the reset transistor is switched off, and a certain cross talk is seen due to the high-low transition of the reset pulse. This cross talk depends on the ratio of the capacitances of the reset switch and the photodiode node. During integration, the photocurrent discharges the capacitance of the photodiode node. Finally, the value is read out through the source follower and the selection transistor. Even if the pixel is shielded from the light and after long integration times, a voltage drop becomes visible due to the dark current that depends on the diode leakage current and leakage of the transistors.

Influence of radiation

The thickness of the sensitive region is about 20 μm. Radiation immunity of CMOS is better than that of CCDs.

The dark current depends on the photodiode, the transistors and the interconnectivity in the pixel. The photodiode leakage current increases steadily with increasing total ionizing dose. This increase arises predominantly from an increased generation at the interface of the silicon and the silicon dioxide. Displacement damage induced by gamma rays is negligible and therefore the bulk dark current is believed to remain constant. The enhanced thermal generation follows from the creation of interface traps with energy levels within the silicon bandgap [12].

2.2.3 Measurement objects and methods

When grabbing images using light covered CCD or CMOS camera there are three types of effects that can be easily measured on the sensors:

- "Hot pixels": permanent and single events,

  There is need to develop algorithm which detect and count white pixels. The algorithm could be similar as star detection algorithm. To recognize single events algorithm should compare white pixels positions on sequence of images.

- Dark current changes

  Dark current changes can be measured by image histogramming.

2.3 Radiation prevention methods

The amount of radiation exposure increases and decreases with the time and distance. The farther away from a radiation source, the less exposure. As a rule, if double the distance, reduce the exposure by a factor of four. Halving the distance, increases the exposure by a factor of four.

The radiation can be reduced with a shielding around a radiation source. Shielding absorbs radiation. The amount of shielding required to protect against different kinds of radiation depends on how much energy they have.

For Alpha a thin piece of light material, such as paper, provides adequate shielding because alpha particles can't penetrate it. Additional covering, for example heavy clothing, is necessary to protect against beta-emitters. Thick, dense shielding, such as lead, is necessary to protect against gamma rays. The higher the energy of the gamma ray, the thicker the lead must be [13], [8].

Neutron radiation shieldings are based on two effects: neutron energy moderation and absorption. As moderator light water or polyethylene plate may be used [2], Thermal neutrons (slow neutrons) are absorbed by cadmium or boron plate [19], [18].

The other method of radiation mitigation of electronics devices is usage chips dedicated to work in irradiation environment or special system design (eg. Triple Module Redundancy) [15], [18], [22], [17].

2.4 Radiation dosimetry using neutron bubble detectors

2.4.1 Neutron bubble detectors

In the experiments were used bubble dosimeters made by BUBBLE TECHNOLOGY INDUSTRIES (BTI). **Figure 2.5** shows clear and exposed to neutrons bubble detector, in **table 2.1** is presented technical specification of used bubble dosimeters [23].

Bubble detectors are very sensitive and accurate neutron dosimeters. Bubble detectors provide instant visible detection and measurement of neutron dose. Inside the detector, tiny droplets of superheated liquid are dispersed throughout a clear polymer. When a neutron strikes a droplet, the droplet immediately vaporizes, forming a visible gas bubble trapped in the gel. The number of droplets provides a direct measurement of the tissue-equivalent neutron dose.

The Bubble Detector is neutron dosimeter where the response is independent of the dose rate and energy, with zero sensitivity to gamma radiation. With an isotropic angular response, neutron dose can be accurately measured regardless of the direction of neutron relative to the

Figure 2.5: Neutron bubble detector [24].

detector [23].

Detector type	BD-PNP	BD100R
Energy Range	200 keV to 15 MeV	200 keV to 15 MeV
Dose Range	0.01 - 50 μSv	0.01 - 50 μSv
Sensitivity	0.033 - 3.3 bub/μSv	0.033 - 3.3 bub/μSv
Automatic Temperature Compensation	Yes	No
Optimum Temperature Range	20 – 37 ^oC	10 – 35 ^oC
Size	145 mm length x 19 mm diameter	120 mm length x 16 mm diameter
Weight	58 g	33 g
Re-use	Yes	Yes
Recompensing Method	Integrated assembly	Integrated assembly
Notes	Recommended for personal neutron dosimetry	Temperature response curve provided

Table 2.1: Bubble detectors, technical specification.

- **BD-PND**

The BD-PND is the recommended detector for personal neutron dosimetry. It incorporates automatic compensation for sensitivity change with temperature over the operational range of 20 – 37 ^oC.

- **BD100R**

  Similar in performance to the BD-PND, but without temperature compensation. A temperature response curve is provided. By controlling detector temperature radiation sensitivity can be increased.

2.5 Specification of Radiation Fields

2.5.1 Radiation environment in Linac II tunnel

Linac II is one of DESY accelerators. It consists of two parts (see **figure 2.6** and **figure 2.7**). First one accelerates electrons produced by 150 *keV* electron source. Electrons with energy about 450 *MeV* hit the tungsten conversion target and produce electron-positron pairs [3]. There are also neutrons and gamma radiation produced as a parasitic radiation. The positrons are stored in Positron Intensity Accumulator (PIA), from where they are distributed to DESY II [15], [18].

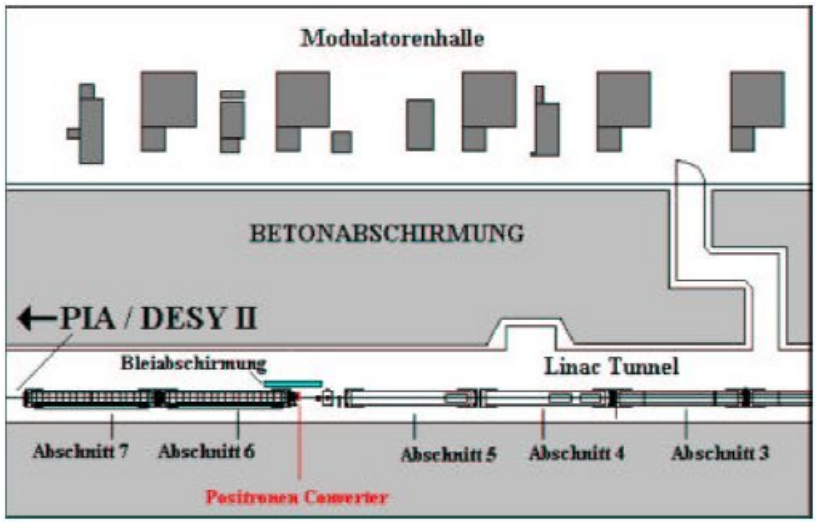

Figure 2.6: Schematic view of Linac II tunnel.

The irradiation environment in Linac II tunnel is not well known. The only value which can help quantify it is PIA current. This current corresponds to number of electrons hitting the converter and to parasitic radiation. The accumulated PIA current (PIA charge) corresponds to total dose of neutrons and gamma. During the experiments Devices Under Tests (DUT)

Figure 2.7: Inside Linac II tunnel.

were placed in various positions along the tunnel (see **figure 2.6**). Changing the distance between the DUT and e^-/e^+ converter allows to change radiation level. Its lowest value is near the entry corridor, about 20 meters from the target and the highest near the converter. It should be pointed that electron-positron converter is placed behind the lead curtain. This shielding reduces fluxes of radiation particles.

2.5.2 Radiation environment in TTF2 tunnel

Phase 2 of the TESLA Test Facility (TTF-2) is planned as a user facility for soft X-ray FEL radiation. The design energy of the electron beam is 1 *GeV*, corresponding to a radiation wavelength of 6.4 *nm* or 194 *eV* photon energy.

The schematic layout of TTF-2 is shown in **figure 2.8**, view inside the tunnel is shown in **figure 2.9**. The electron beam is produced in a RF gun and accelerated up to 1 *GeV* by six cryomodules, each containing eight superconducting RF cavities and a quadrupole doublet. At energy levels of 130 *MeV* and 440*MeV* the electron bunches are compressed from a length of 2 mm RMS at the exit of the gun to approximately 50 μm RMS in order to provide a peak current of 2.5 *kA* required for the FEL. A collimator section protects the FEL undulator by removing particles with an energy deviation larger than $\pm 3\%$ and with large betatron amplitudes. It is also possible to bypass the complete FEL area in order to facilitate machine commissioning and the test of accelerator components. Finally, a dipole magnet deflects the electron beam into a dump, while the FEL radiation propagates to the experimental hall.

The irradiation environment in TTF-2 tunnel is not well known. The only value which

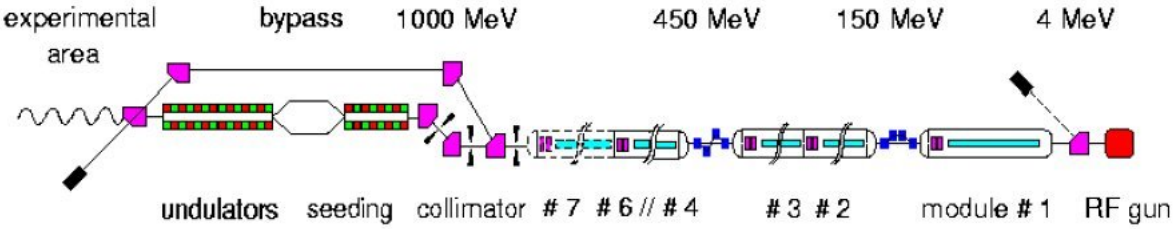

Figure 2.8: Schematic layout of TTF-2.

Figure 2.9: Inside TTF-2 tunnel, module 1.

can help quantify it is Gamma Dose in Ion Chamber. It is proportional to gamma and neutron radiation inside the tunnel.

2.5.3 $^{241}Am/Be$ neutron source

Americium (chemical symbol *Am*) is a man-made radioactive metal. It is produced when plutonium atoms absorb neutrons in nuclear reactors and in nuclear weapons detonations. Americium has several different isotopes, all of which are radioactive. The most important isotope is Am-241. Americium (isotope Am-241) was discovered by nuclear chemist Glenn Seaborg and his colleagues at the University of Chicago in 1944. It is a silver-white, crystalline metal that is solid under normal conditions. Americium-241 primarily emits alpha particles, but also emits gamma rays. A mixture of americium-241 and beryllium emits neutrons. The characteristics of $^{241}Am/Be$ is shown in **table 2.2**.

Common Names:	Americium-241/Beryllium
Chemical Symbol:	Am-241/Be or $^{241}Am/Be$
Atomic Number:	95
Mass Number:	241(146 neutrons)
Chemical Form:	Americium oxide with beryllium metal
Physical Form:	Compressed mixture of americium oxide mixed with beryllium metal.
Physical half-life:	432.2 years
Specific Activity (GBq/g):	127

Table 2.2: Americium-241/Beryllium characteristics.

The spectra of the bare and water moderated neutron source are shown in **figure 2.10** and **figure 2.11**. With a water moderator thickness of 6.25 cm the average neutron energy has dropped from 5.1 MeV to 3.3 MeV (see **figure 2.11**) whereas the neutron flux and dose equivalent rate remained unchanged within that range [2].

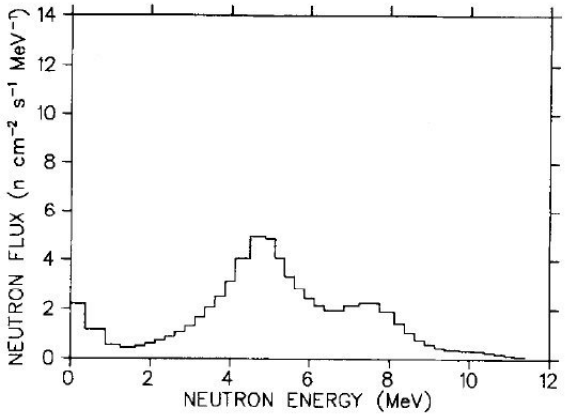

Figure 2.10: Spectrum of $^{241}Am/Be$ neutron source, water moderator thickness 0 *cm*, the average neutron energy E_{av} = 5.1 *MeV* [2].

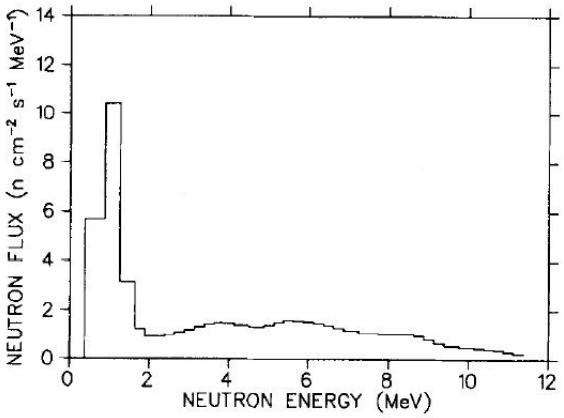

Figure 2.11: Spectrum of $^{241}Am/Be$ neutron source, water moderator thickness 6.25 *cm*, the average neutron energy E_{av} = 3.3 *MeV* [2].

Chapter 3

Project realization

Realization part of the project contain designing and making needed elements of hardware and software layer of the measuring station as well connecting it with commercially available devices with selected sensors.

3.1 Exposure of CCD and CMOS sensors

3.1.1 Irradiation in Linac II tunnel

The measuring station used in Linac II tunnel consists of (see **figure 3.1**):

- PC computer remote controlled by TCP/IP network,
- cameras supply automatic control connected with PC by LPT port,
- CCD and CMOS cameras connected with with PC frame grabber by coaxial cable,

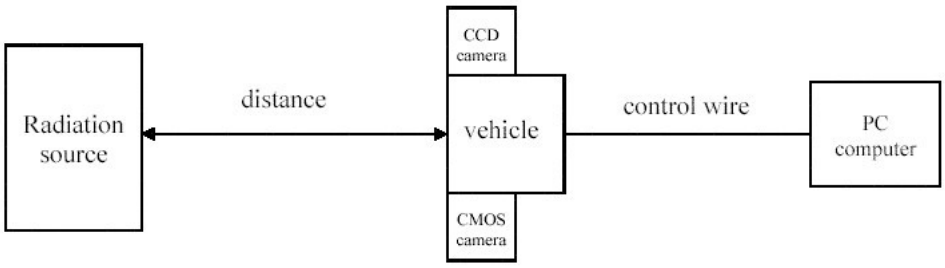

Figure 3.1: The measuring station used in Linac II tunnel.

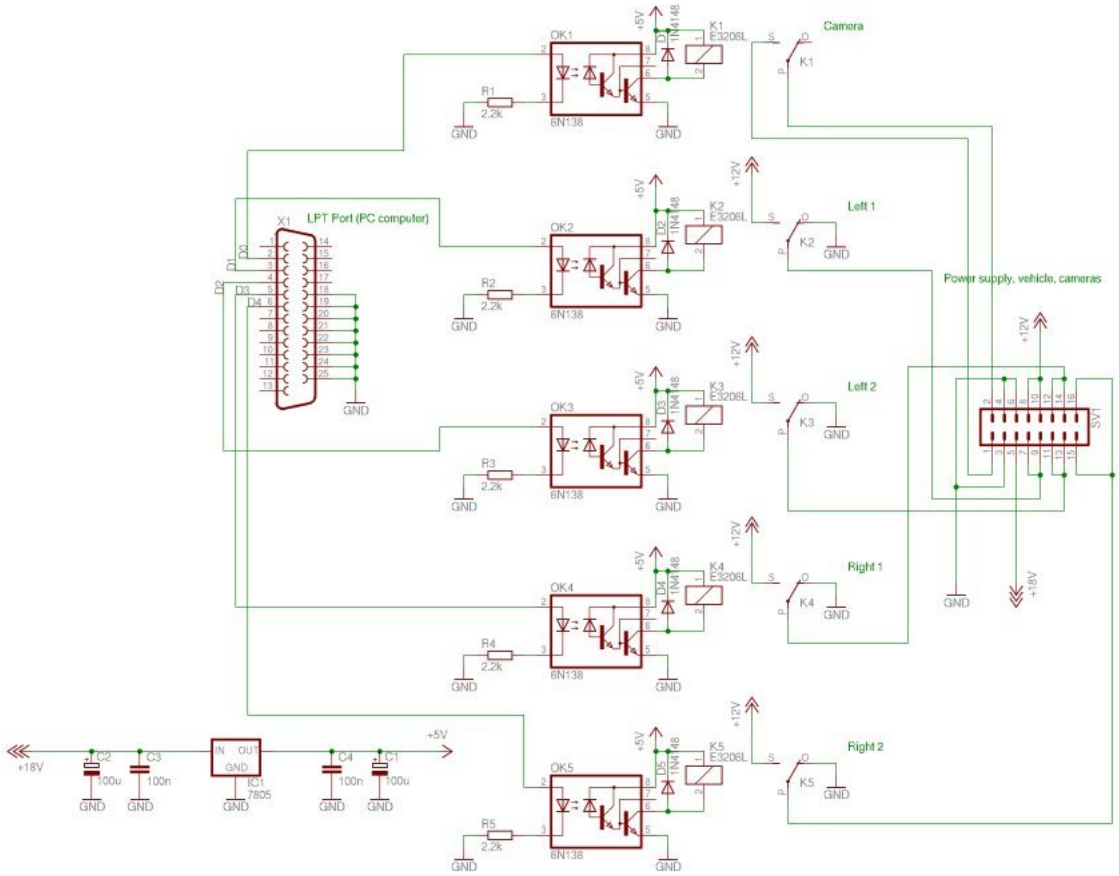

Figure 3.2: Schematic diagram of cameras supply automatic control used in Linac II tunnel.

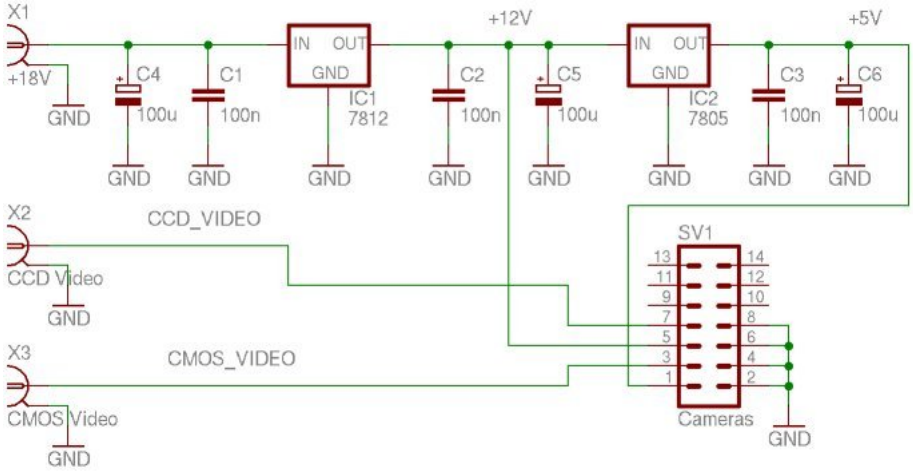

Figure 3.3: Schematic diagram of cameras supply constant-voltage regulator used in Linac II tunnel.

PC computer operates cameras supply control with LPT port. Schematic diagram is shown on **figure 3.2**. For galvanic separation of LPT pins and power supply optotransis-

tor where used. LPT pins switch optotransistor which amplify signal to control electronic relay switching cameras power supply. The CCD and CMOS cameras are connected with PC frame grabber by 50 meters long coaxial cable (50 Ω). To reduce noise and signal clopping constant-voltage regulator was used with the cameras (schematic diagram is shown on **figure 3.3**). Radiation level was changing by changing distance between cameras and radiation source – position converter, see schematic view of Linac II tunnel, **figure 2.6**. In the experiment where used CCD-Camera-Modules available in CONRAD (Best.-Nr. 11 67 50), sensor size 500 [H] x 582 [V] pixels (291000 pixels).

3.1.2 Irradiation with the $^{241}Am/Be$ source

The measuring station used with $^{241}Am/Be$ source is shown on **figure 3.4**. As a neutron source was used $^{241}Am/Be$. Cameras were put in different distance form the source: 6.5 cm and 13 cm. Water moderator thickness was 0 cm, 6.5 cm or 13 cm, with or without *Cd* shielding. Cameras where connected to PC's frame grabber. In the experiment where used CCD-Camera-Modules available in CONRAD (Best.-Nr. 11 67 50), sensor size 500 [H] x 582 [V] pixels (291000 pixels).

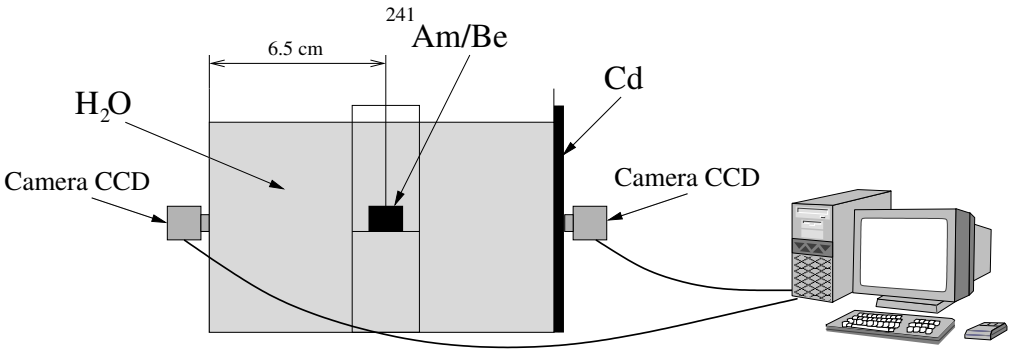

Figure 3.4: The measuring station used with $^{241}Am/Be$ source.

3.1.3 Irradiation at TTF-2 tunnel

The measuring station used TTF-2 tunnel is shown on **figure 3.5**, it was build with three CCD cameras:

- without any cover,
- covered by a boron plate (4 *mm* thick),
- covered by a *Cd* plate (1.5 *mm* thick) and put in polyethylene box (40 *mm* thick).

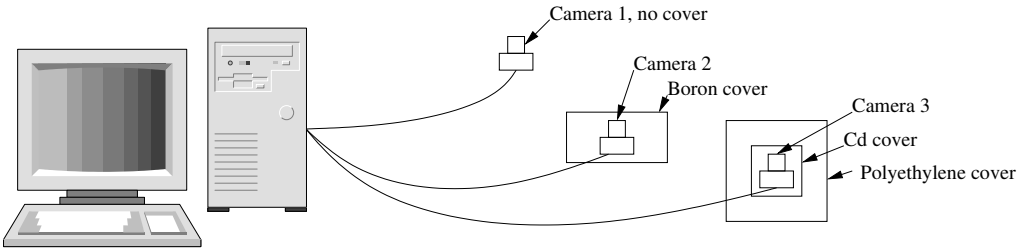

Figure 3.5: The measuring station used TTF-2 tunnel.

Cameras were connected to PC's frame grabber with long coaxial cables. In the experiment where used CCD-Camera-Modules available in CONRAD (Best.-Nr. 11 67 50), sensor size 500 [H] x 582 [V] pixels (291000 pixels).

3.2 Algorithms for detecting and counting effects formed in CCD and CMOS sensors under the influence of irradiation

The software works on LINUX operating system, is written mainly in C/C++ also shell scripts, TCL/TK scripts, Perl. For image grabbing it uses **bttv** or **pwc** frame grabber module (V4L interface).

3.2.1 Detecting hot pixels

White pixels detection using simple bright pixels thresholding was not sufficient, therefore the algorithm was based on stars detecting algorithm. It consists of the following steps [14]:

- Grab an image from a camera (the camera was light covered), it boils down to a few subsequent actions:
  - Opening V4L device (eg. `/dev/video0`).

    The device is operated by **bttv** module – for cameras with PCI framegrabber card, or **pwc** module – for USB Philips cameras. The drivers meet the **V4L** (Video For Linux, version 1) standard, in this way the camera is visible from the level of the **Linux** user as a `/dev/video0` device.
  - Loading a structure that describes the device properties.
  - Setting the desired window size.

  - Read the image.

    A buffer filed with binary data. In YUV format for Philips cameras and RGB for cameras with framegrabber PCI card.

  - Convert RGB or YUV image (format depends on used camera) to BW format.

  Setting and loading webcam parameters is performed with `ioctl()` function calls with appropriate parameters. **Pwc** and **bttv** modules give the possibility of mapping a device for a specific area of operational memory (using the `mmap()` function).

- Find hot pixels (white pixels).

  The image is stored in an object in the form of a table called **basic table**. Recognition of bright pixels consists of:

  - finding a local luminosity maximum

  Finding the local luminosity maxim is performed in a working table, which is created by multiplying the basic table by square matrix (Gauss matrix), performing the role of a filter sharpening the image. Its elements are created according to this formula:

$$C_{kl} = \frac{e^{-\frac{(k-r)^2+(l-r)^2}{2(0,4246\cdot fwhm)^2}}}{2\pi(0,4246\cdot fwhm)^2}$$

  where:
  C_{kl} – an element of the matrix with k, l coordinates,
  r – matrix radius,
  $fwhm$ – half-width of the profile.

  Next, the matrix is additionally normalized and brought to a form where the sum of the elements (volume) equals zero:

$$C'_{kl} = \frac{C_{kl}}{s} - \frac{1}{d^2}$$

$$s = \sum_{k=0}^{d}\sum_{l=0}^{d} C_{kl}$$

$$d = 2r+1$$

  where:
  C'_{kl} – new element of the matrix with k, l coordinates,

C_{kl} – old element of the matrix with k, l coordinates,
r – matrix radius.

Elements of the working table are calculated according to the following formula:

if $F_{ij} \leq threshin$ then:

$$W_{ij} = 0$$

in other case:

$$W_{ij} = \sum_{k-0}^{d} \sum_{l=0}^{d} F_{i-r+k,j-r+l} C_{kl}$$

$$d = 2r + 1$$

where:
W_{ij} – element of the working table,
F_{ij} – element of the basic table,
C_{kl} – element of the filtering matrix,
r – filtering matrix radius,
$threshin$ – background threshold, should be equal to: *arithmetic mean of pixel luminosity + 3 * standard deviation*

Next, for each element of the working table (with the exception of pixels from the frame border) W_{ij} the condition if $W_{ij} > threshold$ is checked and whether W_{ij} is a local maximum. Objects thus found are hot pixels.

- Count hot pixels.
- Store the number and list of positions in a file.
- Draw diagram which presents number of hot pixels during the experiment.

3.2.2 Detecting permanent and single event effects

Detecting permanent and single event effects algorithm is based on comparison between sequence of hot pixels position lists. The algorithm consists of the following steps:

- sort lists by time,

- read two followed lists,
- compare hot pixels positions from first list with positions from second list (maximal displacement: 2 pixels), hot pixels which are on both lists are permanent damages, others are single event effects,
- count and store the numbers and dates,
- repeat for next lists,
- at the end draw diagrams which presents number of permanent damages and single events effects during the experiment.

3.2.3 Detecting dark current and noise level changes

Detecting dark current and noise level changes is based on image histogram. When camera is covered maximum of black image histogram is mean value of dark current. If dark current rises the histogram maximum moves to higher values (brighter pixels).

3.2.4 Software implementation

The software is based on star detecting algorithms developed by author for **AudeLa** project. It works on LINUX operating system, is written mainly in C/C++ also shell scripts, TCL/TK scripts, Perl. For image grabbing uses **bttv** frame grabber module (V4L interface).

Algorithm operates on single image, image series and images directly grabbed from a camera. The images are saved in **FITS** format. This is flexible format which allows to add to file header any needed keywords like date, distance from the converter, camera type etc. Grabbed images can be saved on a hard disc for future usage.

Found hot pixels number and list of positions can be saved in text files. Later used for detecting permanent and single event effects.

Figure 3.6 shows hot pixels detected by algorithm.

3.3 Construction of the irradiation rig for the neutron bubble detector

Construction of measuring station for the neutron bubble detector is shown on **figure 3.7**. It's composed of:

- neutron bubble detector (bubble dosimeter),

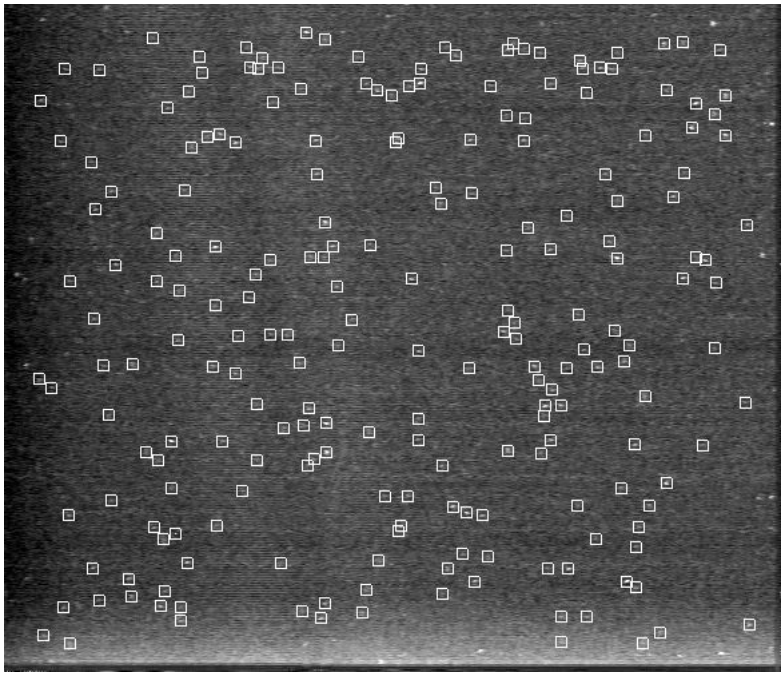

Figure 3.6: Detected hot pixels.

- USB CMOS camera with photographic lens, 58 mm,
- lightbox to illuminate neutron bubble detector,
- wooden stand,
- everything covered with a carton box,
- PC computer connected with camera with USB cable.

3.4 Algorithm for automatic reading of bubble dosimeter dose

Algorithm for automatic reading of bubble dosimeter dose is based on image processing: detecting bubbles edges, recognize bubble, eliminate non bubble objects and count bubbles.

3.4.1 Bubble recognition and counting

Bubble recognition and counting algorithm:

- read image,

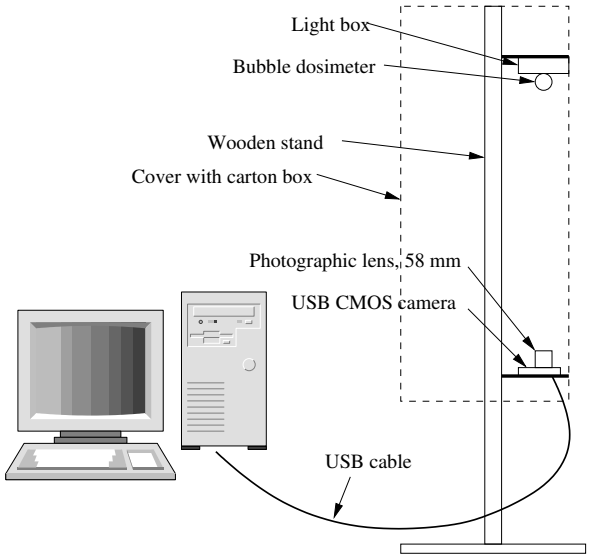

Figure 3.7: Neutron bubble detector test system.

- detect edges with Canny edge detection algorithm:
  - smooth the image with Gaussian filter to eliminate any noise,
  - find the image gradient to highlight regions with high spatial derivatives,
  - track along these regions and suppresses any pixel that is not at the maximum,
  - reduce gradient array by hysteresis,
  - track along the remaining pixels that have not been suppressed,
  - hysteresis uses two thresholds and if the magnitude:
    - is below the first threshold,
      - then it is set to zero (non-edge),
    - is above the high threshold,
      - then it is made an edge,
    - is between the 2 thresholds,
      - then it is set to zero unless there is a path from this pixel to a pixel with a gradient above T2,
- eliminate straight lines and small objects,
- count bubbles.

3.4.2 On-line analysis

On-line analysis is extension of bubble recognition and counting algorithm. Every few seconds image was taken from camera and processed with bubble recognition and counting algorithm and results saved in a file.

3.4.3 Software implementation in JAVA, OBCA v1

The software is written in JAVA Swing, it is named **OBCA** v1 – Optical Bubble Counting Algorithm. The software can read any type of image (jpg, bmp, etc.) and runs on any operating system with JRE. Its graphical user interface is shown on **figure 3.8**. First step is **Read image** then **Edge detection**, **Count bubbles**. In any case image can be saved as **BMP**.

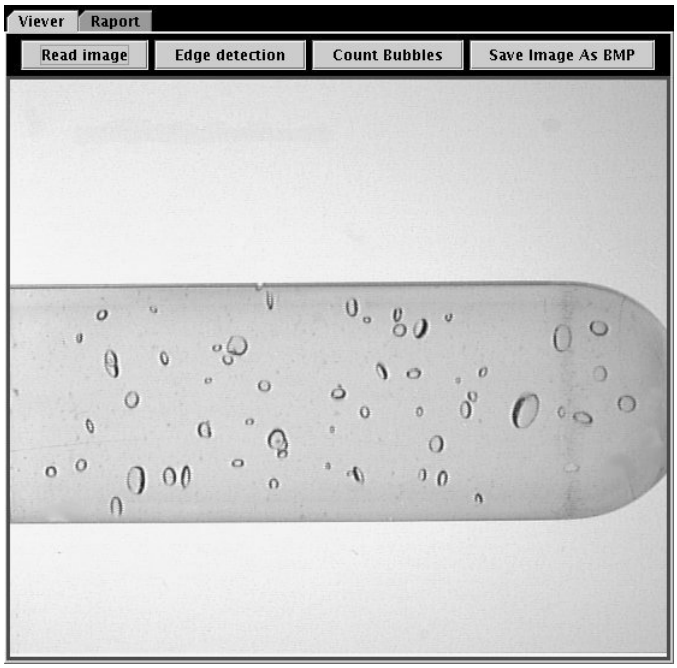

Figure 3.8: OBCA, read image.

Chapter 4

Irradiation investigation

In the research section set working and testing of particular parts and whole measuring station with the software will be carried out using chosen commercially available CCD and CMOS sensors in accelerator's irradiation environment at DESY.

4.1 CCD and CMOS sensors tests results

4.1.1 Tests in Linac II accelerator tunnel

- **Number of hot pixels during the experiment.**

  One of defects happened by irradiation CCD sensors are hot pixels. To show dependence between number of hot pixels and total integrated dose the values where drew on the same figure (see **figure 4.1** and **figure 4.2**). Integral PIA current is equivalent of total integrated dose. Number of hot pixels rises when there is PIA current – integral of PIA current rise (see **figure 4.1**).

  To check nature of hot pixels power supply of CCD sensors was switch on and switch off (0 hot pixels – camera switched off, **figure 4.1**). The number of hot pixels quickly increases after switch on and stops on permanent level (see **figure 4.2**). This is example of theoretically predicted **bulk damage** and shows that hot pixels are permanent defects.

- **Image histogram, "dark current" during the experiment.**

  Other defect happened during irradiation of CCD and CMOS sensors is "dark current" increase. It was observed during the experiment. Maximum of histogram moved to right and staid wider (see **figures 4.3 – 4.6**). It confirms theoretically predicted **surface damage**.

- **Number of hot pixels in function of total integrated dose.**

  To use a CCD sensor as a radiation sensor estimation of number of hot pixels in function of total integrated dose was done. Deltas of number of hot pixels where counted, then count integral and draw diagram in function of integral PIA current (see **figure 4.7**).

  It seems to be a linear dependence, hence approximated with a first degree polynomial (see **figure 4.7**).

  $$pix = 0.000119 \cdot pia + 0.0332$$

  where:

  pix - integral deltas of number of hot pixels [percents],

  pia - integral PIA current.

  Calibration with LED diodes shows total integrated dose was:

  $$1.81 \cdot 10^{11} \frac{neutrons}{cm^2}$$

  Simply count shows that dose $0.4 \cdot 10^{11} \frac{neutrons}{cm^2}$ cause 0.1 percent increase of number of hot pixels.

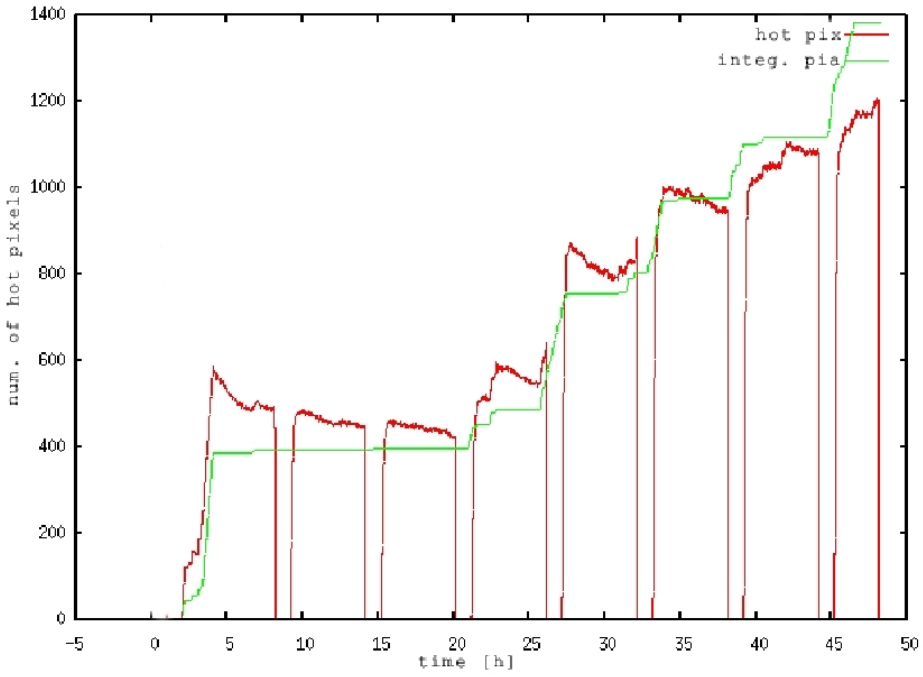

Figure 4.1: Number of hot pixels on CCD camera and integral of PIA current.

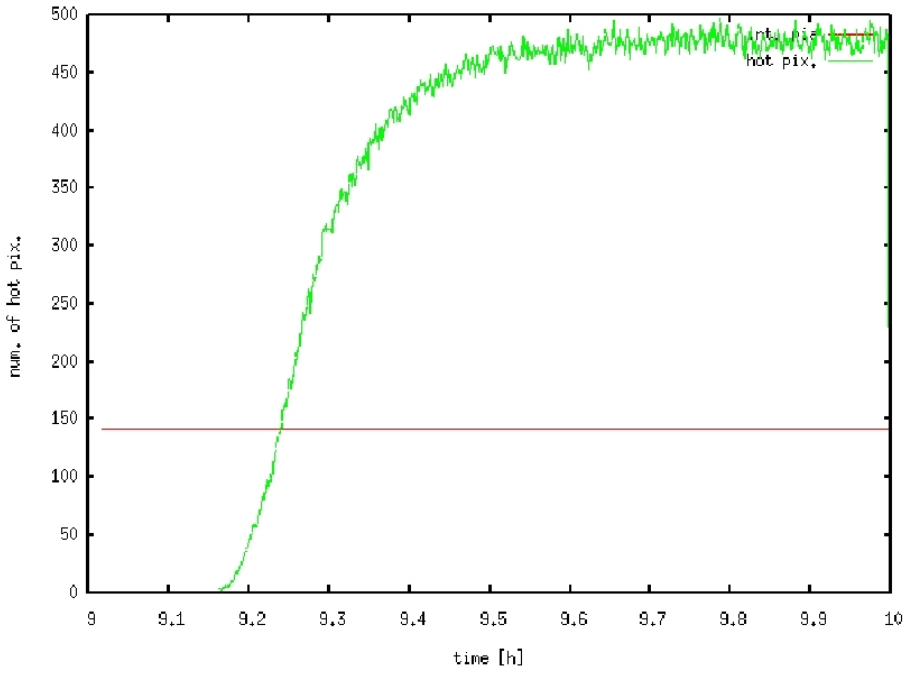

Figure 4.2: Number of hot pixels on CCD camera after "power on", no PIA current.

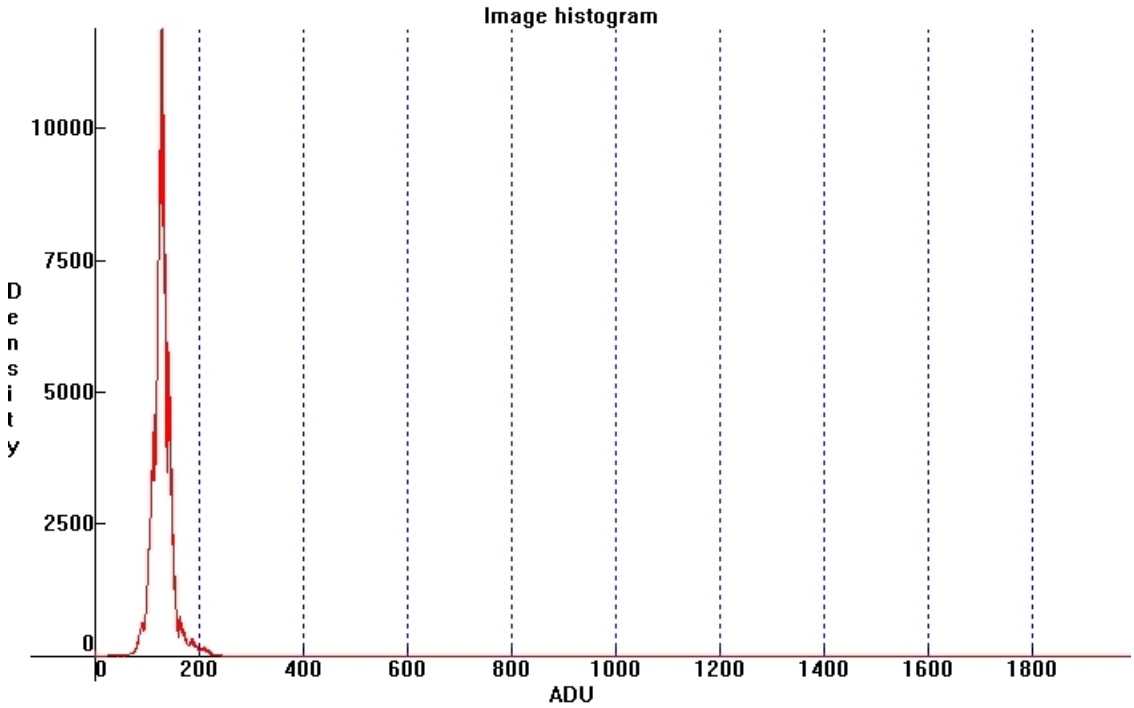

Figure 4.3: Histogram of CCD signal output after 3.5 hours.

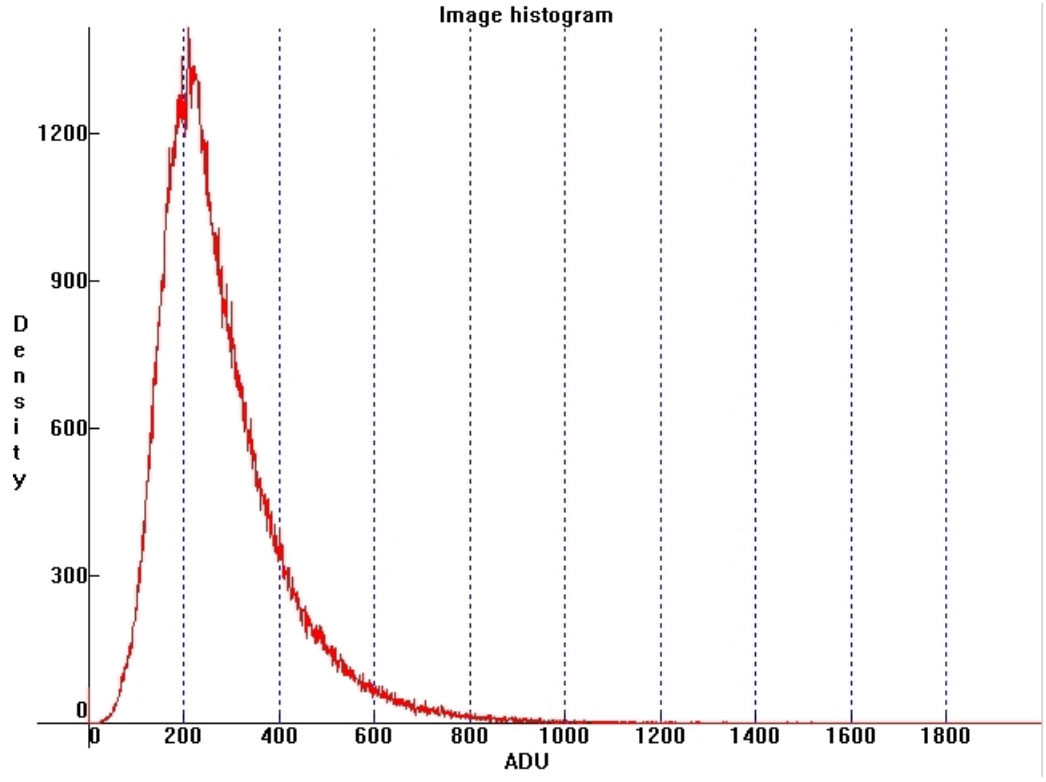

Figure 4.4: Histogram of CCD signal output after 9 days.

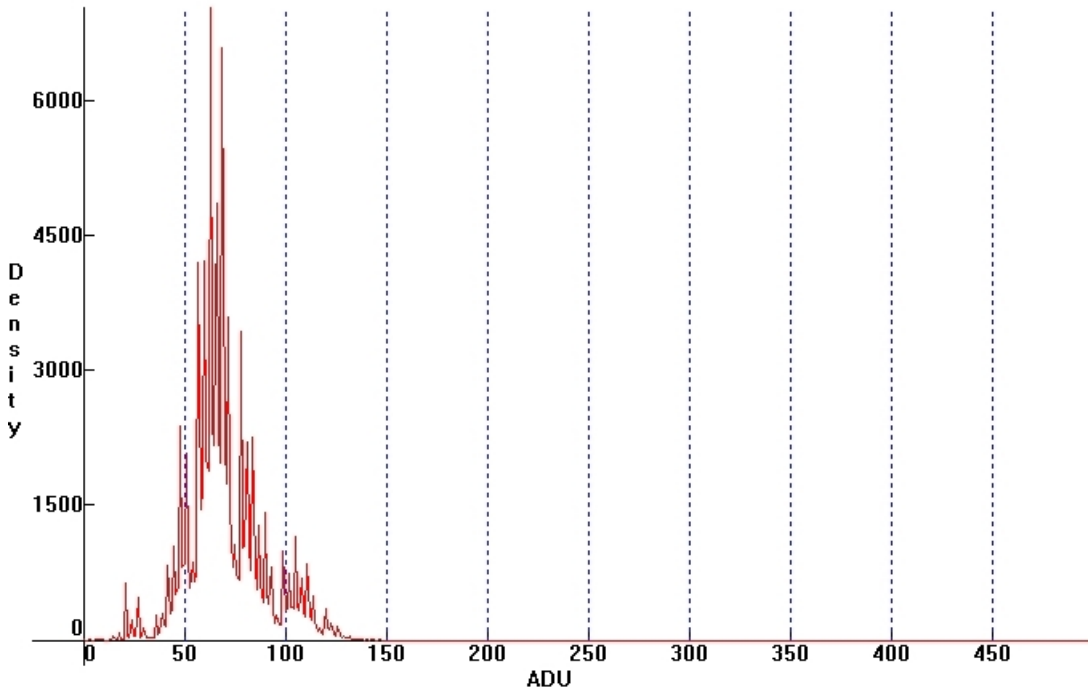

Figure 4.5: Histogram of CMOS signal output after 3.5 hours.

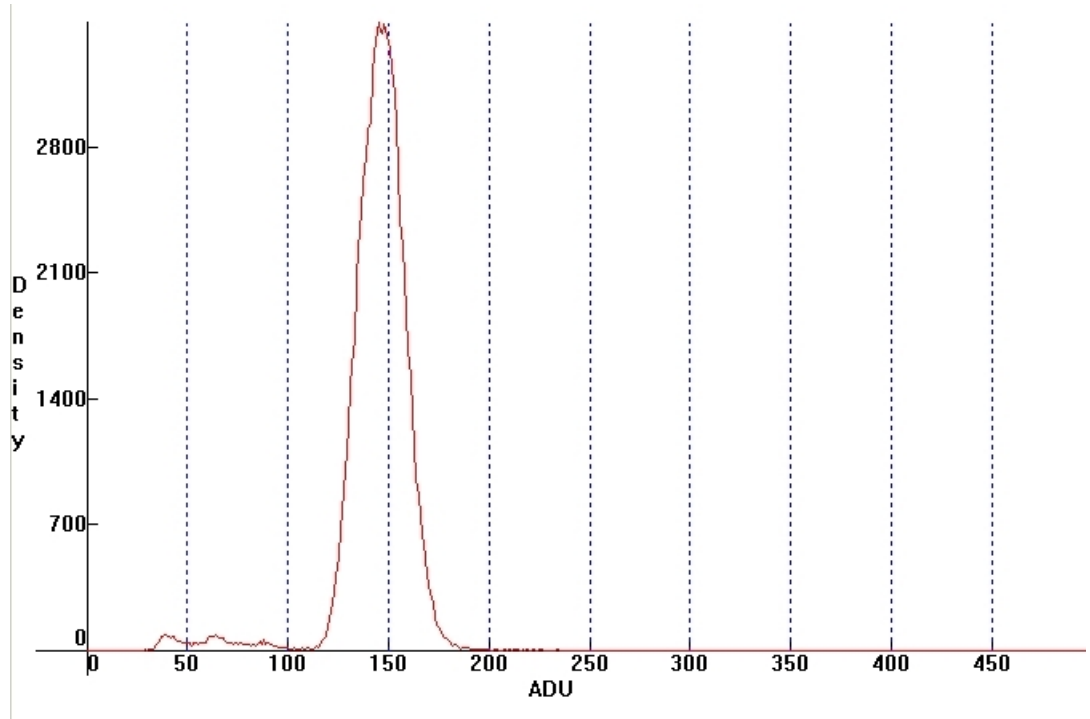

Figure 4.6: Histogram of CMOS signal output after 9 days.

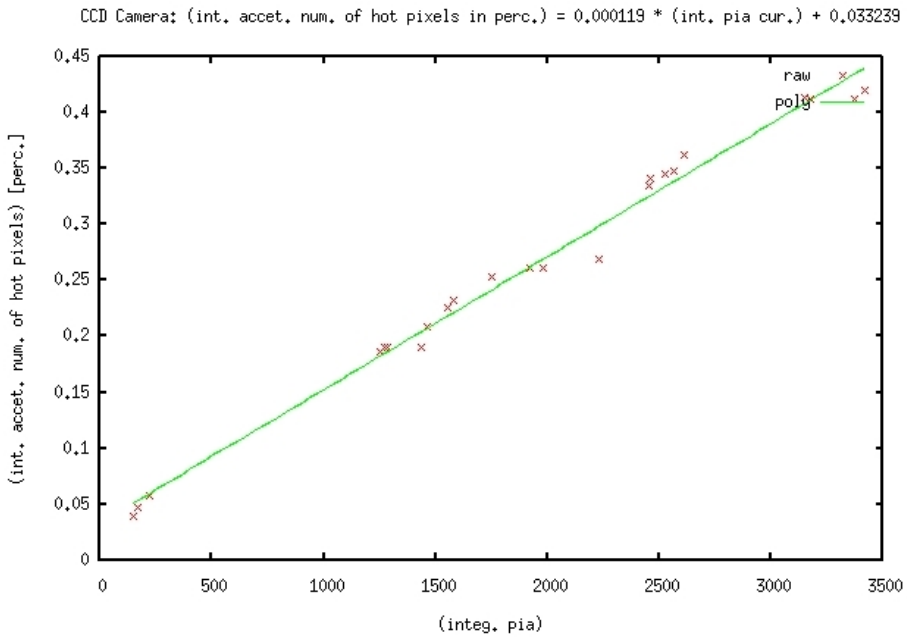

Figure 4.7: Integral deltas of number of hot pixels as a function of integral PIA current.

4.1.2 Investigation of SEU and permanent damage on commercial CCD cameras induced by moderated and unmoderated neutrons from a $^{241}Am/Be$ source

The results are presented in the table and figures 4.8 – 4.10. Figures show number of permanent and single event defects in function of time. Numbers where averaged by 10 (10 seconds).

Fig.	dist.	H_2O	Cd	source m	dos. m	dos. nr	bub.	$\mu Sv/b$	μSv	per.	SEU
4.8	6.5	-	-	30	-	-	-	-	-	12	7
4.9	6.5	6.5	-	20	10	169602	35	7.8	273	2	6
4.10	6.5	6.5	+	30	10	169577	42	7.2	302.4	3	0.5
	13	13	-	10	10	169774	15	7.2	108	0	1.5
	13	6.5	+	10	10	170070	17	8.4	142.8	0	0.4
	13	6.5	-	10	10	170377	16	6.1	97.6	0	2

Table 4.1: Results of investigation of SEU and permanent damage on commercial CCD cameras induced by moderated and unmoderated neutrons from a $^{241}Am/Be$ source.

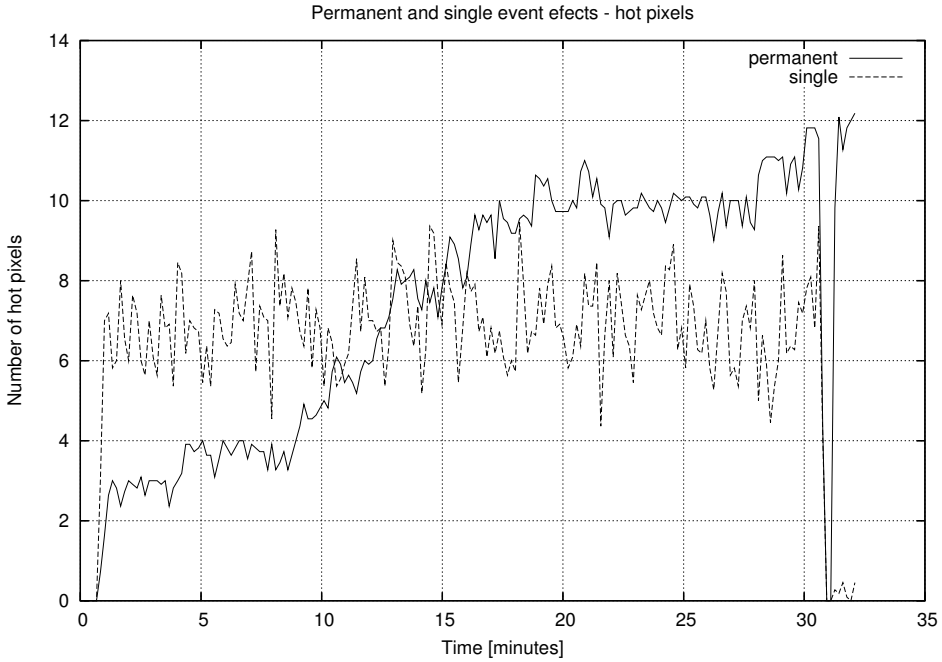

Figure 4.8: CCD, distance 6.5 cm, no water, no Cd, no dosimeter, source for 30 min.

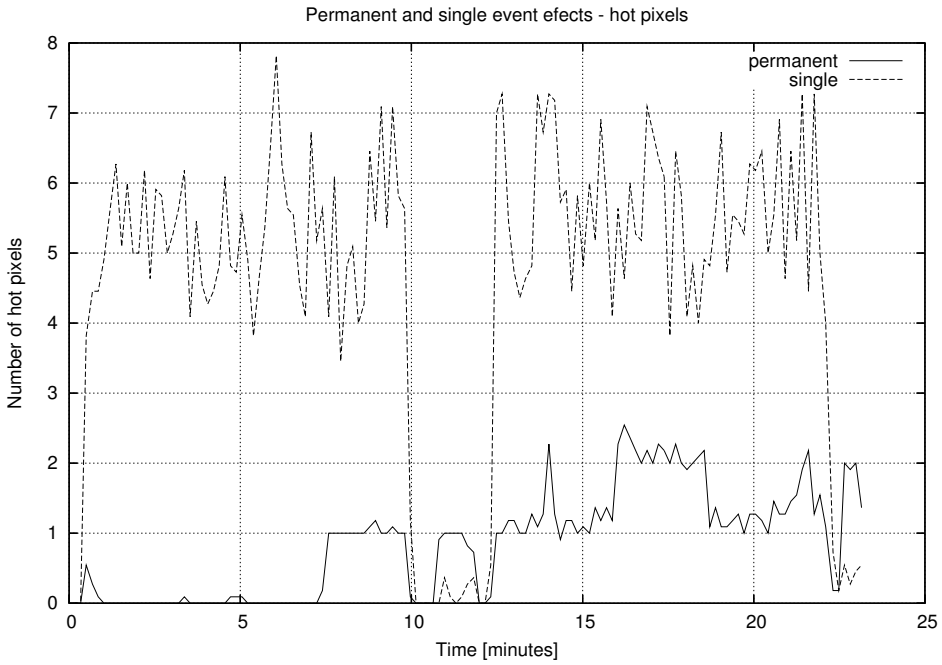

Figure 4.9: CCD, distance 6.5 cm, water 6.5 cm, no Cd, dosimeter 169602 - 35 bubbles, dose 273 μSv (for 10 min.), source for 20 min.

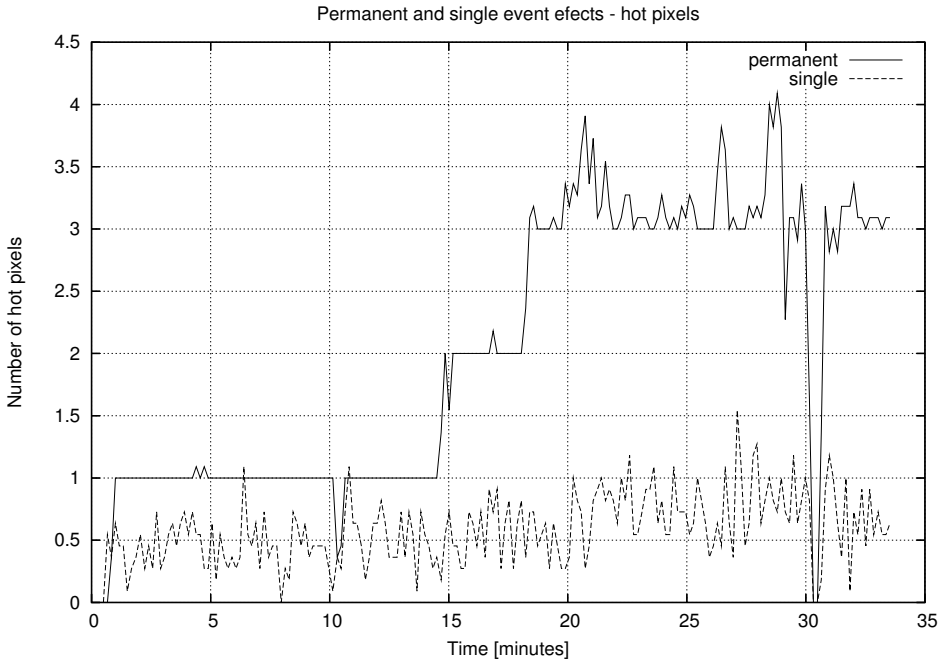

Figure 4.10: CCD, distance 6.5 cm, water 6.5 cm, with Cd, dosimeter 169577 - 42 bubbles, dose 302.4 μSv (for 10 min.), source for 30 min.

4.1.3 Tests in TTF-2 accelerator tunnel

Figure 4.11 shows Gamma Dose in Ion Chamber. Because of problems with measuring device there are some time gaps in data downloaded from TTF logs: eg. between 80 - 250 minutes. **Figure 4.12** shows "hot pixels" on camera without cover, after 377 minutes in TTF2 tunnel. Number of permanent damages SEU's after 560 minutes of experiment are shown in **table 4.2**.

Camera cover	permanent	SEU's/frame
–	14	4
boron	4	10
Cd and polyethylene	5	5

Table 4.2: Permanent and SEU's after 560 minutes of the experiment.

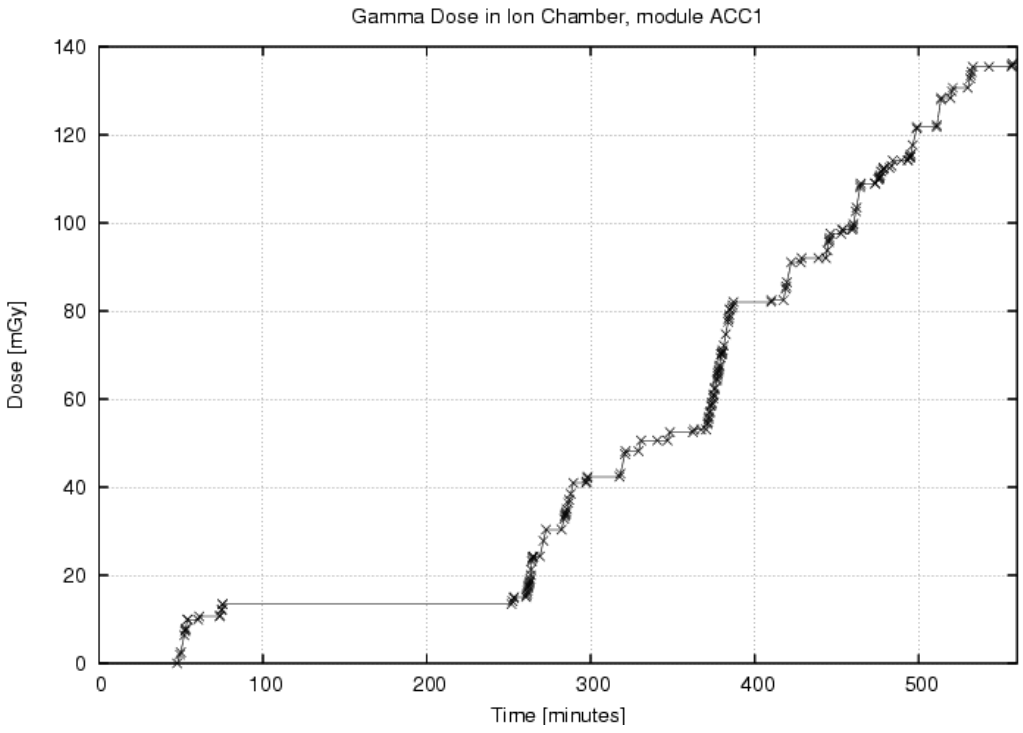

Figure 4.11: Gamma Dose in Ion Chamber.

4.2 Research on Optical Bubble Counting Algorithm

There were tested bubble dosimeters made by BUBBLE TECHNOLOGY INDUSTRIES (BTI). **Figure 4.13** shows bubble dosimeter exposed to neutrons. Radiation dose is linear function

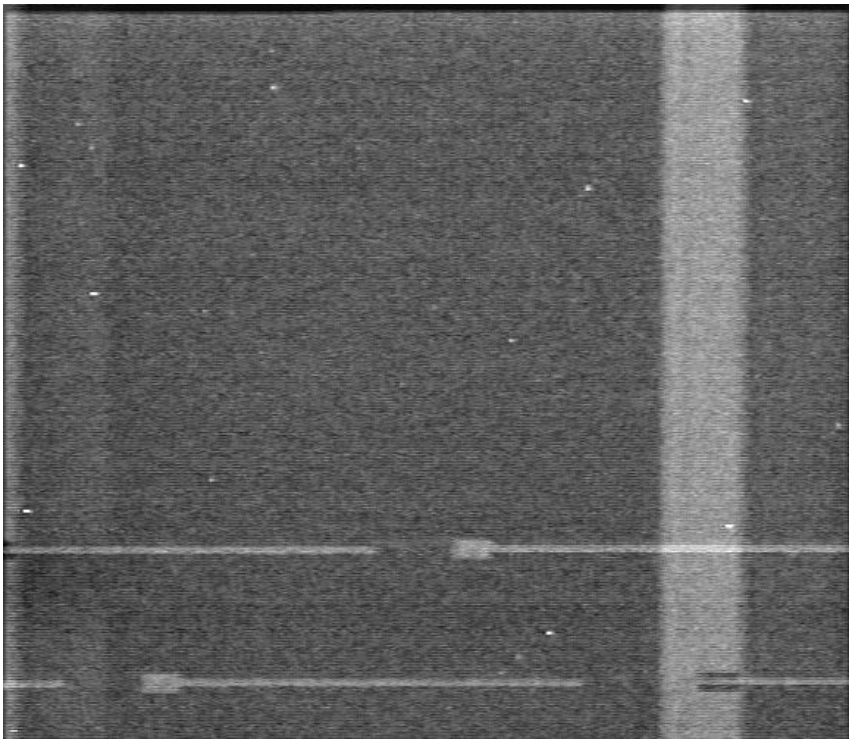

Figure 4.12: Hot pixels on camera without cover after 377 minutes in TTF2 tunnel.

of number of bubbles in the dosimeter. The are presented results of testing automatic bubble counting algorithm.

Figure 4.13: Bubble dosimeter, nr 170070.

4.2.1 Single image reading

Figure 4.14 shows interesting fragments of two sides of bubble dosimeter, **figure 4.15** image with detected edges and **figure 4.16** with eliminated straight lines. Number of bubbles counted manually is **82** and automatically **80**. Other comparison between manual and automatic counting is shown in the **table 4.3**.

Method/Angle	0/360 ^{o}	90 ^{o}	180 ^{o}	270 ^{o}	Average	Diff. (%)
Manual 1	227	220	217	245	227.45	4.5
Manual 2	227	232	247	293	249.75	-4.9
Manual 3	209	242	260	249	240	-0.8
OBCA v 1	252	223	227	239	235.25	1.2

Table 4.3: Comparison between manual and automatic counting.

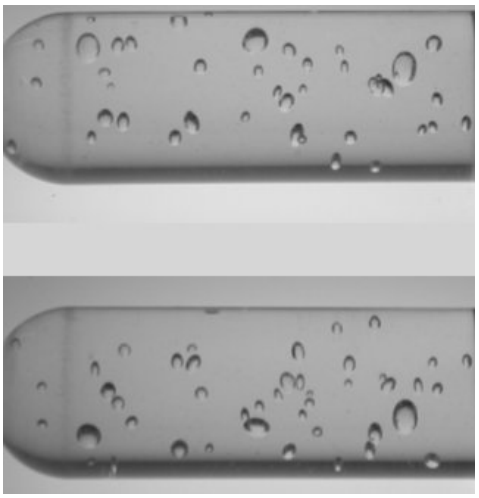

Figure 4.14: Bubble dosimeter, nr 170070, interesting fragment.

4.2.2 On-line reading

Neutron bubble detectors were irradiated by neutrons from a $^{241}Am/Be$ source in three different conditions:

- $^{241}Am/Be$ source,
- $^{241}Am/Be$ source, 6.5 cm water moderator,
- $^{241}Am/Be$ source, 6.5 cm water moderator, boron shielding.

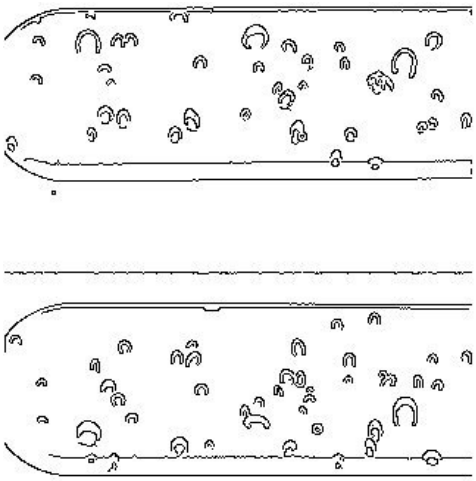

Figure 4.15: Bubble dosimeter, nr 170070, after Canny filter - edges detected.

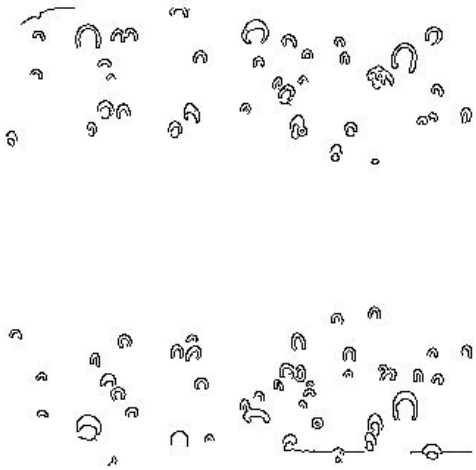

Figure 4.16: Bubble dosimeter, nr 170070, straight lines eliminated.

Distance between the source and neutron bubble detectors was $1m$, irradiation time was $24h$. Three different dosimeters where used.

Figure 4.17 shows number of bubbles during the experiments, figures 4.18 – 4.20 shows dose equivalent during the experiments.

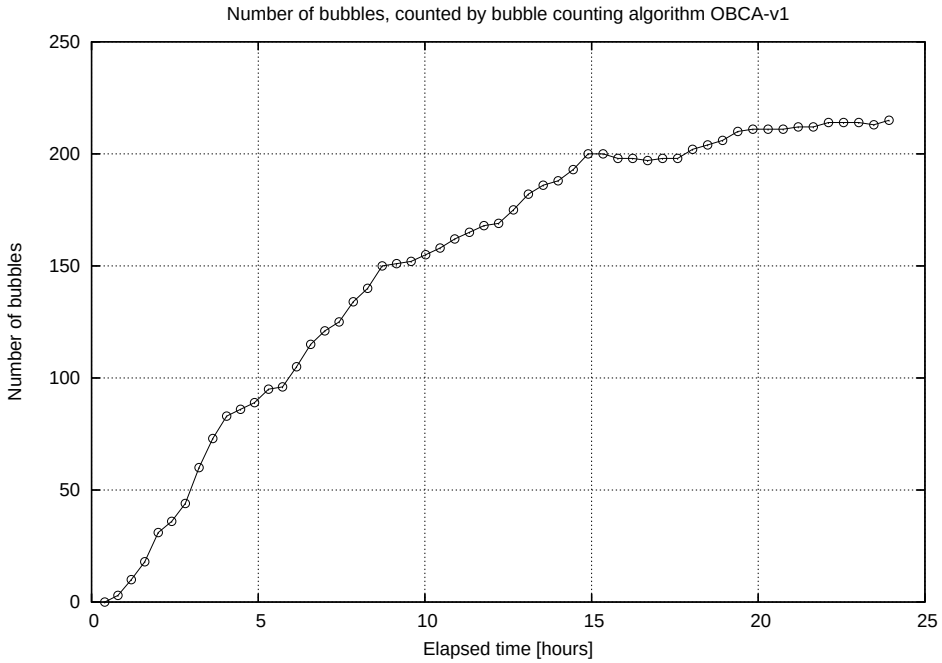

Figure 4.17: Number of bubbles, $^{241}Am/Be$ source. Bubble dosimeter nr 170070.

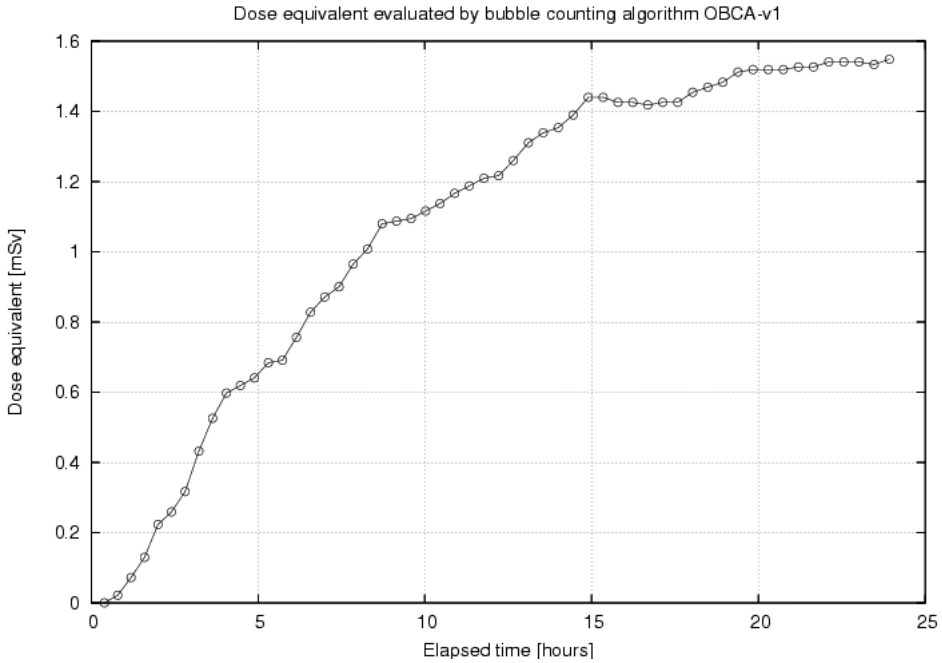

Figure 4.18: Dose equivalent, $^{241}Am/Be$ source. Bubble dosimeter nr 170070.

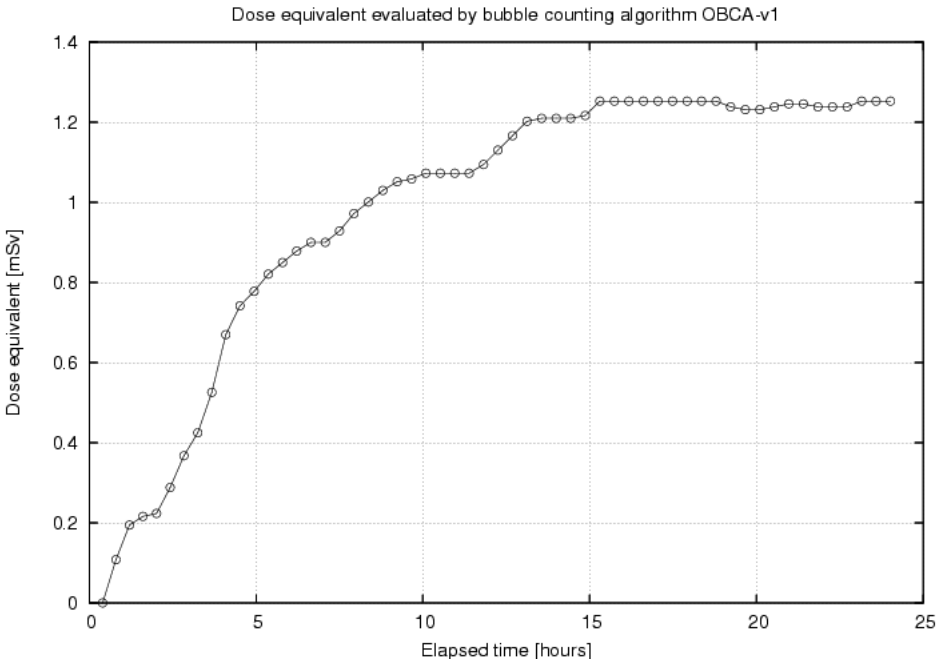

Figure 4.19: Dose equivalent, $^{241}Am/Be$ source, water. Bubble dosimeter nr 169774.

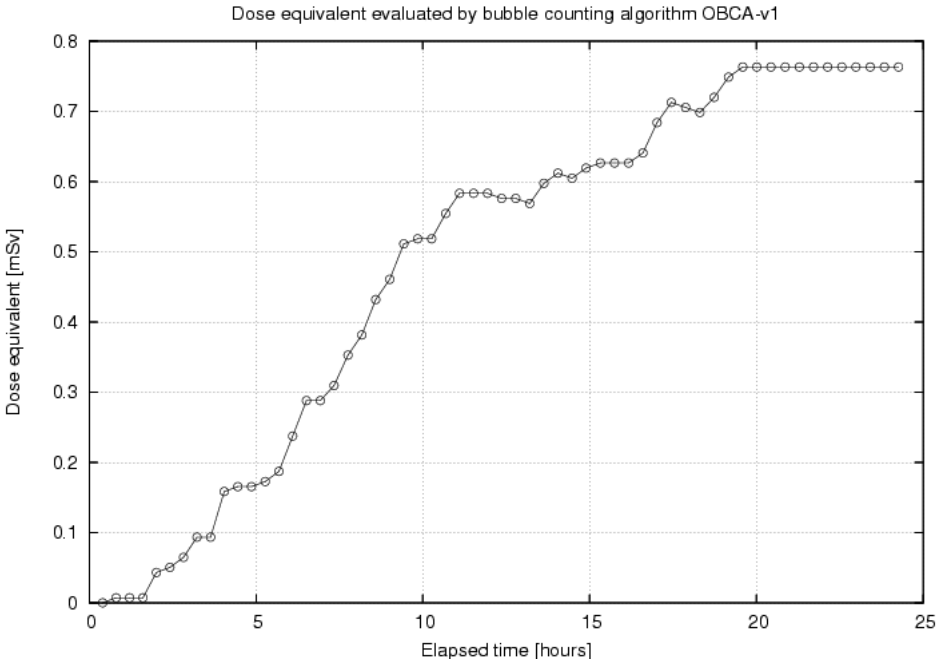

Figure 4.20: Dose equivalent, $^{241}Am/Be$ source, water, boron. Bubble dosimeter nr 194140.

Chapter 5

Conclusions and summary

All experiments show radiation causes damages of electronic devices. These damages can be automatically recognized and counted. Obtained information make possible building radiation detection and measurement systems based on Charge Coupled Devices and CMOS sensors.

The errors are mainly caused by neutrons. Gamma radiation limits devices lifetime. The results of experiments shows that some radiation mitigation methods are possible. Tested conventional shieldings like: **polyethylene**, **boron** or **cadmium** can be used as radiation protection of electronics operating in the accelerator's tunnel. The other method is usage chips dedicated to work in irradiation environment or special system design (eg. Triple Module Redundancy).

5.1 Experiments with CCD and CMOS sensors

Neutron radiation exposure of CCD and CMOS cameras sensors:

- Causes increase number of permanent "hot pixels" (known as "dark current spikes") manifest themselves as pixels with much higher dark current than the average value for the CCD.
- Single Event Upsets visible as "blinking white pixels".
- Causes average dark current increase, observed by analyzing image histogram.

Model of neutron radiation detector based on CCD sensors was build. The number of permanent damages is linear function of radiation dose. It was pr oven that integrated dose $0.4 \cdot 10^{11} \frac{neutrons}{cm^2}$ cause increase 0.1% number of "hot pixels" on the sensor.

The automatic online monitoring software occurred quite efficient but sensitive on noise. The main amount of noise came from 50 *m* long coaxial cable and digital to analogue conversion (to video signal) used in cameras (this problem could be solved by using USB cameras instead). High level of noise from CMOS camera caused improper work of algorithm, not all "hot pixels" where found.

Neutron radiation shieldings are based on two effects: neutron energy moderation and absorption. The average energy of neutrons emitted by $^{241}Am/Be$ source can be dropped from 5.1 *MeV* to 3.3 *MeV* with light water moderator thickness of 6.5 *cm* [2]. Maximum of neutron flux moved to low energy. Moderation with polyethylene plate causes similar effects. Thermal neutrons (slow neutrons) are absorbed by cadmium or boron plate.

Water moderation reduce number of permanent defects on CCD sensors, see **figures 4.8** and **4.9**. It proves permanent defects are caused by fast neutrons.

SEU are caused by thermal neutrons (low energy), which can be stopped by *Cd* or boron shielding, see **figure 4.10**.

5.2 Optical Bubble Counting Algorithm

The algorithm occurred quite efficient and accurate, as was shown in **table 4.3**. Difference between number of bubbles automatically and manually counted was similar, about a few percents. It is less accurate when processing low resolution images and images with many overlapping bubbles – saturation effect.

Model of online bubble monitoring device was build and tested at TTF-2 tunnel and with $^{241}Am/Be$ neutron source.

First version of the algorithm was written in C/C++ and Perl scripts, able to capture images from a camera and real time bubble monitoring. The software wasn't suppled with GUI interface. Version written in JAVA has user friendly GUI interface, reads many types of image files and is independent on operating system.

5.3 Scope of usage and propositions of future development

Neutron radiation detector based on CCD sensors can be used as low cost and real time radiation detection device. The software can be developed and suppled with user friendly GUI.

OBCA software is convenient automatic neutron bubble detector reader, can be used for single image reading as well for real time reading. Development of bubble recognition

method should provide 3D recognition, based on two angles images – rotated dosimeter or images from two cameras. JAVA version may be suppled with camera interface to read image directly.

Appendix A

Health Physics Aspects

Radioactive materials that decay spontaneously produce ionizing radiation, which has sufficient energy to strip away electrons from atoms (creating two charged ions) or to break some chemical bonds. Any living tissue in the human body can be damaged by ionizing radiation. The body attempts to repair the damage, but sometimes the damage is too severe or widespread, or mistakes are made in the natural repair process. The most common forms of ionizing radiation are alpha and beta particles, or gamma and X-rays.

The annual dose limit for members of the general public is 1 *mSv*, for nuclear energy workers is 20 *mSv*.

A.1 Health effects occur from exposure to radionuclides

In general, the amount and duration of radiation exposure affects the severity or type of health effect. There are two broad categories of health effects: stochastic and non-stochastic.

A.1.1 Stochastic Health Effects

Stochastic effects are associated with long-term, low-level (chronic) exposure to radiation. Increased levels of exposure make these health effects more likely to occur, but do not influence the type or severity of the effect.

Cancer is considered by most people the primary health effect from radiation exposure. Simply put, cancer is the uncontrolled growth of cells. Ordinarily, natural processes control the rate at which cells grow and replace themselves. They also control the body's processes for repairing or replacing damaged tissue. Damage occurring at the cellular or molecular level, can disrupt the control processes, permitting the uncontrolled growth of cells – cancer. This is why ionizing radiation's ability to break chemical bonds in atoms and molecules makes it such a potent carcinogen.

Other stochastic effects also occur. Radiation can cause changes in DNA, the "blueprints" that ensure cell repair and replacement produces a perfect copy of the original cell. Changes in DNA are called mutations.

Sometimes the body fails to repair these mutations or even creates mutations during repair. The mutations can be teratogenic or genetic. Teratogenic mutations affect only the individual who was exposed. Genetic mutations are passed on to offspring.

A.1.2 Non-Stochastic Health Effects

Non-stochastic effects appear in cases of exposure to high levels of radiation, and become more severe as the exposure increases. Short-term, high-level exposure is referred to as 'acute' exposure.

Many non-cancerous health effects of radiation are non-stochastic. Unlike cancer, health effects from 'acute' exposure to radiation usually appear quickly. Acute health effects include burns and radiation sickness. Radiation sickness is also called 'radiation poisoning'. It can cause premature aging or even death. If the dose is fatal, death usually occurs within two months. The symptoms of radiation sickness include: nausea, weakness, hair loss, skin burns or diminished organ function.

A.2 Radiation Protection Basics

A.2.1 Time

The amount of radiation exposure increases and decreases with the time people spend near the source of radiation.

A.2.2 Distance

The farther away people are from a radiation source, the less their exposure. As a rule, if double the distance, reduce the exposure by a factor of four. Halving the distance, increases the exposure by a factor of four.

A.2.3 Shielding

The greater the shielding around a radiation source, the smaller the exposure.

Shielding simply means having something that will absorb radiation between body and the source of the radiation. The amount of shielding required to protect against different kinds of radiation depends on how much energy they have.

For Alpha a thin piece of light material, such as paper, provides adequate shielding because alpha particles can’t penetrate it. Additional covering, for example heavy clothing, is necessary to protect against beta-emitters. Some beta particles can penetrate and burn the skin. Thick, dense shielding, such as lead, is necessary to protect against gamma rays. The higher the energy of the gamma ray, the thicker the lead must be.

Appendix B

Publications during the study

1. Arkadiusz Kalicki, Lech Mankiewicz, Krzysztof Pozniak, Grzegorz Wrochna *Sky Eye. Image processing software for amateur astronomers*, Proceedings of SPIE.
2. Arkadiusz Kalicki *SkyEye, Users manual*, EU-HOU project.
3. D. Rybka, A. Kalicki, K. Pozniak, R. Romaniuk, B. Mukherjee, S. Simrock, *Irradiation Investigations for TESLA and X-FEL experiments at DESY*, Proceedings of SPIE, Volume 5775,pp. 78-95
4. D. Rybka, A. Kalicki, K. Pozniak, R. Romaniuk, B. Mukherjee, S. Simrock, *Development of a Digital Photometer for the Evaluation of COTS LED Fast Neutron Dosimeter*, Proceedings of SPIE (being published)
5. D. Rybka, A. Kalicki, K. Pozniak, R. Romaniuk, B. Mukherjee, S. Simrock, *Irradiation Investigations for TESLA and X-FEL experiments at DESY*, Proceedings of SPIE, Volume 5948.
6. B. Mukherjee, D. Rybka, A. Kalicki, S. Simrock, R. Romaniuk, *Radiation Effects on Electronics Located in High-Energy Accelerator Environment*, Proceedings of SPIE, Volume 5948.
7. B. Mukherjee, D. Rybka, A. Kalicki, S. Simrock, R. Romaniuk, *Development of a Neutron KERMA Dosimeter Using Low Cost Gallium Arsenide Light Emitting Diodes*, Proceedings of SPIE (being published)
8. J. Zysik, A. Kalicki, J. Szewiński: *MOSIX cluster construction and testing with OBCA*. Proceedings of SPIE, Volume 5948.

List of Figures

List of Tables

Bibliography

[1] G. Materlik, Th. Tschentscher: *TESLA Technical Design Report. PART V, THE X-RAY FREE ELECTRON LASER.*

[2] B. Mukherjee: *Development of a Simple Neutron Irradiation Facility with Variable Avarage Energy Using a Light Water Moderated* ^{241}*Am/Be source*. Nuclear Instruments and Methods in Physics Research A 363 (1995), pp. 616-618

[3] H. Weise: *Introduction to Linac 2 / PIA and Linac 3*. 2003

[4] L. Dusseau: *Introduction to Radiation Issues of Commercial-Off-The-Shelf (COTS) Components*. CERN Training 2000

[5] M. Dentan: *Radiation Effects on Electronic Components and Circuits*. CERN Training 2000

[6] K. Bunkowski, I. Kassamakov, K. Kierzkowski, M. Kudla, T. Maenpaa, K. Pozniak, D. Rybka, E. Tuominen, D. Ungaro, W. Zabolotny: *Irradiation Effects in Electronic Components of the RPC Trigger for the CMS Experiments*. SPIE Proceedings, Volume 5484

[7] F. Gusmao: *Single Event Upset Mitigation Techniques for Programmable Devices*

[8] J. Burnham: *Radiation Protection ("Green Book")*

[9] Particle Physics Experiments at JLC ACFA Linear Collider Working Group Report

[10] Investigation of radiation damage effects in neutron irradiated CCD. Physics Department, University of Oregon

[11] Datasheets of used devices, chips and parts

[12] J. Bogaerts, B. Dierickx: *Total Dose Effects on CMOS Active Pixel Sensors*.

[13] U.S. Environmental Protection Agency: *Understanding Radiation*. www.epa.gov.

[14] Arkadiusz Kalicki *SkyEye, Users manual*. EU-HOU Project

[15] D. Rybka, A. Kalicki, K. Pozniak, R. Romaniuk, B. Mukherjee, S. Simrock: *Irradiation Investigations for TESLA and X-FEL experiments at DESY*. Proceedings of SPIE, Volume 5775, pp. 78-95

[16] D. Rybka, A. Kalicki, K. Pozniak, R. Romaniuk, B. Mukherjee, S. Simrock: *Development of a Digital Photometer for the Evaluation of COTS LED Fast Neutron Dosimeter*. Proceedings of SPIE (being published)

[17] K. Bunkowski, I. Kassamakov, K. Kierzkowski, M. Kudla, T. Maenpaa, K. Pozniak, D. Rybka, E. Tuominen, D. Ungaro, G.Wrochna,W. Zabolotny: *Radiation Tests of CMS RPC Muon Trigger Electronic Components*. Nuclear Instruments and Methods in Physics Research A 538 (2005), pp. 708-717

[18] D. Rybka, A. Kalicki, K. Pozniak, R. Romaniuk, B. Mukherjee, S. Simrock: *Irradiation Investigations for TESLA and X-FEL experiments at DESY*. Proceedings of SPIE, Volume 5948.

[19] B. Mukherjee, D. Rybka, A. Kalicki, S. Simrock, R. Romaniuk: *Radiation Effects on Electronics Located in High-Energy Accelerator Environment*. Proceedings of SPIE, Volume 5948.

[20] J. Zysik, A. Kalicki, J. Szewiński: *MOSIX cluster construction and testing with OBCA*. Proceedings of SPIE, Volume 5948.

[21] B. Mukherjee, D. Rybka, A. Kalicki, S. Simrock, R. Romaniuk: *Development of a Neutron KERMA Dosimeter Using Low Cost Gallium Arsenide Light Emitting Diodes*. Proceedings of SPIE (being published)

[22] M. Dentan: *Radiation Effects on Electronic Components and Circuits*. CERN Training 2000

[23] Bubble Technology Industries (BTI) website: *www.bubbletech.ca*.

[24] Bubble Technology Industries: *Defender, Neutron Detector*.

[25] Interactions News webpage: *Start of Free-Electron Laser at DESY*. www.interactions.org.

[26] DESY, Deutsches Elektronen Synchrotron webpage: *www.desy.de*.

[27] TESLA, Tera Electron Volt Superconducting Linear Accelerator webpage: *tesla.desy.de*.

[28] Federal Ministry of Education and Research: *XFEL - the European X-Ray Laser Project*.

[29] E. Plönjes: *VUV-FEL User Facility at DESY*. HASYLAB, Deutsches Elektronen-Synchrotron DESY, Hamburg, Germany.

[30] Joachim Ullrich: *Matter in Brilliant Light: The VUV Free Electron Laser*. Max Planck Institute for Nuclear Physics.

[31] J. Feldhaus, E. Saldin, E. Schneidmiller, M. Yurkov: *Seeding plans and experiments at the DESY VUV-FEL*. Workshop on the Physics of Seeded FELs, MIT.

[32] Reinhard Brinkmann: *The European X-ray FEL, Accelerator Layout*. LINAC2004, Lübeck.

[33] Reinhard Brinkmann: *XFEL Project Overview*.

[34] A VUV Free Electron Laser at the TESLA Test Facility at DESY: *Conceptual Design report*. Deutsches Elektronen-Synchrotron, DESY, TESLA-FEL 95-03, DESY, Hamburg, Germany.

[35] HASYLAB: *FEL Basics: FEL vs. Optical Laser*. Webpage www-hasylab.desy.de.

[36] Welt der Physik: *Röntgenlaser XFEL*. www.weltderphysik.de.

[37] Gordon R. Hopkinson: *Radiation Effects on a Radiation Tolerant CMOS Active Pixel Sensor*.

[38] James E. Brau, Nikolai Sinev: *Operation of a CCD particle detector in the presence of bulk neutron damage*. Physics Department, University of Oregon, Eugene, OR 97403-1274, USA.

[39] James E. Brau, Olga B. Igonkina, Chris T. Potter, Nikolai B. Sinev: *Investigation of Radiation Damage in the SLD CCD Vertex Detector*. 2003 IEEE Nuclear Science Symposium, Medical Imaging Conference, and Workshop of Room-Temperature Semiconductor Detectors.

[40] James E. Brau, Olga B. Igonkina, Chris T. Potter, Nikolai B. Sinev: *Investigation of radiation damage effects in neutron irradiated CCD*. Computer Physics Communications.